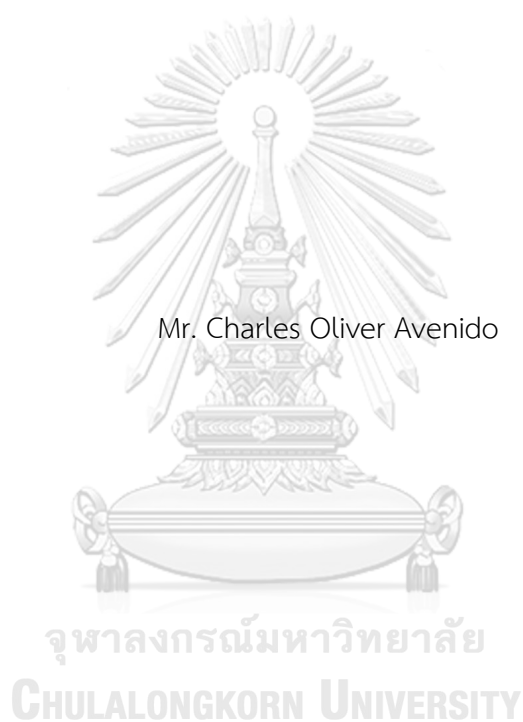


ENZYME-FREE HYDROGEN PEROXIDE SENSOR FROM DUAL-SHAPED PLASMONIC SILVER  
NANOPARTICLES



A Thesis Submitted in Partial Fulfillment of the Requirements  
for the Degree of Master of Science in Chemistry  
Department of Chemistry  
FACULTY OF SCIENCE  
Chulalongkorn University  
Academic Year 2022  
Copyright of Chulalongkorn University

ไฮโดรเจนเปอร์ออกไซด์เซ็นเซอร์แบบไมโครเอ็นไซม์จากอนุภาคพลาสมาโพลิเมอร์นาโนสองรูปร่าง



วิทยานิพนธ์นี้เป็นส่วนหนึ่งของการศึกษาตามหลักสูตรปริญญาวิทยาศาสตรมหาบัณฑิต

สาขาวิชาเคมี ภาควิชาเคมี

คณะวิทยาศาสตร์ จุฬาลงกรณ์มหาวิทยาลัย

ปีการศึกษา 2565

ลิขสิทธิ์ของจุฬาลงกรณ์มหาวิทยาลัย

Thesis Title ENZYME-FREE HYDROGEN PEROXIDE SENSOR FROM  
DUAL-SHAPED PLASMONIC SILVER NANOPARTICLES  
By Mr. Charles Oliver Avenido  
Field of Study Chemistry  
Thesis Advisor Assistant Professor Dr. MONPICHAR SRISA-ART  
Thesis Co Advisor Associate Professor Dr. KANET WONGRAVEE

---

Accepted by the FACULTY OF SCIENCE, Chulalongkorn University in Partial  
Fulfillment of the Requirement for the Master of Science

..... Dean of the FACULTY OF SCIENCE  
(Professor Dr. POLKIT SANGVANICH)

THESIS COMMITTEE

..... Chairman  
(Professor Dr. SANONG EKGASIT)

..... Thesis Advisor  
(Assistant Professor Dr. MONPICHAR SRISA-ART)

..... Thesis Co-Advisor  
(Associate Professor Dr. KANET WONGRAVEE)

..... Examiner  
(Associate Professor Dr. APICHAT IMYIM)

..... External Examiner  
(Dr. Tewarak Parnklang)

ชาร์ล โอลิเวอร์ อาเวนิโด : ไฮโดรเจนเปอร์ออกไซด์เซ็นเซอร์แบบไมโซนาโนจากอนุภาคพลาสมอนิกซิลเวอร์นาโนสองรูปร่าง. ( ENZYME-FREE HYDROGEN PEROXIDE SENSOR FROM DUAL-SHAPED PLASMONIC SILVER NANOPARTICLES) อ.ที่ปรึกษาหลัก : มนพิชา ศรีสะอาด, อ.ที่ปรึกษาร่วม : คณศ วงษ์ระวี

งานวิจัยนี้ได้พัฒนาริธีตรวจวัดไฮโดรเจนเปอร์ออกไซด์รูปแบบใหม่โดยใช้ซิลเวอร์นาโนสเฟียร์ (silvernanospheres, AgNSs) ร่วมกับซิลเวอร์นาโนปริซึมที่หุ้มด้วยซิเตรต (citrate-capped silvernanoprisms, citrate-capped AgNPrs) เนื่องจากไฮโดรเจนเปอร์ออกไซด์มีสมบัติเฉพาะที่สามารถออกซิไดซ์อนุภาคนาโนเงินและยังสามารถรีดิวโลหะเงิน ทำให้สามารถพัฒนาเซ็นเซอร์ AgNSs/AgNPrs ที่มีความจำเพาะสูงสำหรับการตรวจวัดไฮโดรเจนเปอร์ออกไซด์ โดยไฮโดรเจนเปอร์ออกไซด์จะออกซิไดส์ AgNSs เกิดเป็นซิลเวอร์ไอออน ซึ่งจะถูกรีดิวซ์โดยไฮโดรเจนเปอร์ออกไซด์ เกิดเป็นโลหะเงินซึ่งจะเกาะบน AgNPrs เนื่องจาก AgNPrs ถูกหุ้มด้วยซิเตรต ทำให้การโตของ AgNPrs จะเกิดเฉพาะด้านข้าง ทำให้ AgNPrs มีขนาดใหญ่ขึ้น ส่งผลให้สเปกตรัมเกิดการเลื่อนไปทางสีแดง (red shift) และการเพิ่มขึ้นของค่าการดูดกลืนแสง (absorbance) ของแถบอินเพลนไดโพลพลาสมอนเรโซแนนซ์ (in-plane dipole plasmon resonance, IPDPR) ดังนั้นจะเห็นการเปลี่ยนสีของเซ็นเซอร์จากสีเหลือง สีส้ม สีแดง สีม่วง และสีน้ำเงิน ในการวิเคราะห์เชิงปริมาณของไฮโดรเจนเปอร์ออกไซด์จะใช้การวิเคราะห์อัตราส่วน (ratiometric analysis) ค่าการดูดกลืนแสงที่แถบไดโพลพลาสมอนเรโซแนนซ์ (DPR) ที่ลดลงของ AgNSs และค่าการดูดกลืนแสงที่ IPDPR ที่เพิ่มขึ้นของ AgNPrs ซึ่งได้ขีดจำกัดการตรวจวัดไฮโดรเจนเปอร์ออกไซด์เข้มข้นเท่ากับ 4.8 ไมโครโมลาร์ การศึกษาความจำเพาะของเซ็นเซอร์ต่อการตรวจวัดไฮโดรเจนเปอร์ออกไซด์ โดยได้ทำทดสอบกับแอนไอออนชนิดต่าง ๆ พบว่าเซ็นเซอร์สามารถทนต่อการรบกวนจากโบรไมด์และไอโอดิไดได้ในระดับไมโครโมลาร์ ซึ่งจะไม่เกิดปัญหาการรบกวนถ้าใช้เซ็นเซอร์ในการวิเคราะห์ตัวอย่างน้ำจืดหรือตัวอย่างทางชีวภาพที่มีปริมาณโบรไมด์และไอโอดิไดในระดับต่ำ นอกจากนี้ยังได้พัฒนาเซ็นเซอร์สำหรับการตรวจวัดปริมาณของ  $H_2O_2$  ที่เจือจางในสารละลาย โดยทำการปรับอัตราส่วนความเข้มข้นของเซ็นเซอร์ AgNSs/NPrs พบว่าที่อัตราส่วน 20:10 ppm สามารถใช้ในการตรวจวัดปริมาณ  $H_2O_2$  ที่เจือจางในสารละลายได้ และการเปลี่ยนสีของเซ็นเซอร์ AgNSs/NPrs จะชัดเจนมากขึ้น เมื่อใช้ความเข้มข้นของเซ็นเซอร์ที่สูงขึ้น ซึ่งพบว่าเซ็นเซอร์ที่พัฒนาขึ้นสามารถวิเคราะห์ปริมาณของไฮโดรเจนเปอร์ออกไซด์ได้ในช่วงความเข้มข้นที่กว้างตั้งแต่ 10 ถึง 800 mM การทดสอบความแม่นยำและความเที่ยงของเซ็นเซอร์ที่พัฒนาขึ้นโดยการตรวจวัดปริมาณไฮโดรเจนเปอร์ออกไซด์ในน้ำดื่ม พบว่าความแม่นยำและความเที่ยงการวิเคราะห์อยู่ในระดับที่ยอมรับได้ ดังนั้นเซ็นเซอร์ AgNSs/NPrs ที่พัฒนาขึ้นจึงเป็นทางเลือกที่น่าสนใจ

สาขาวิชา เคมี ปลายมือชื่อนิสิต .....

ปีการศึกษา 2565 ปลายมือชื่อ อ.ที่ปรึกษาหลัก .....

ปลายมือชื่อ อ.ที่ปรึกษาร่วม .....

# # 6372028523 : MAJOR CHEMISTRY

KEYWORD: hydrogen peroxide sensor silver nanoparticles nanoprisms growth-based sensing colorimetric detection

Charles Oliver Avenido : ENZYME-FREE HYDROGEN PEROXIDE SENSOR FROM DUAL-SHAPED PLASMONIC SILVER NANOPARTICLES. Advisor: Asst. Prof. Dr. MONPICHAR SRISA-ART Co-advisor: Assoc. Prof. Dr. KANET WONGRAVEE

A novel growth-based strategy for the determination of hydrogen peroxide has been developed using a mixture of silver nanospheres (AgNSs) and citrate-capped silver nanoprisms (AgNPrs). The unique ability of hydrogen peroxide to oxidize silver nanoparticles and reduce silver metal consequently was exploited to produce a highly sensitive and selective sensor (AgNSs/NPrs). Citrate-capping of the AgNPrs only allows the lateral growth that resulted in a red shift and intensity enhancement of the in-plane dipole plasmon resonance (IPDPR) band. Consequently, distinct hues from yellow, orange, red, purple to blue were produced from the diluted sensors. Ratiometric analysis was employed to quantify  $H_2O_2$  using absorbance values at the decreasing dipole plasmon resonance (DPR) band of the AgNSs and the increasing IPDPR of the AgNPrs. A detection limit of  $4.8 \mu M$  was achieved with concentrated hydrogen peroxide determination. Selectivity of the sensor was evaluated using common anions. According to the results of the interference testing, the sensor can only tolerate micromolar levels of bromide and iodide which is not an issue for fresh water or biological samples. The detection of diluted  $H_2O_2$  was further simplified by using an optimized AgNSs/NPrs sensor concentration and ratio of 20:10 ppm. Colorimetric readout can be achieved at higher sensor concentrations that also provides a broad linear range from 10 to 800 mM. Accuracy and precision testing on concentrated hydrogen peroxide and spiked drinking water show excellent results. Thus, growth-based sensing using dual-shaped silver nanoparticles is a promising alternative as it enables a quick, highly selective, and sensitive colorimetric determination of hydrogen peroxide with high accuracy and precision.

Field of Study: Chemistry

Student's Signature .....

Academic Year: 2022

Advisor's Signature .....

Co-advisor's Signature .....

## ACKNOWLEDGEMENTS

First, I would like to express my sincerest gratitude to my advisors Assistant Professor Dr. Monpichar Srisa-Art and Associate Professor Dr. Kanet Wongravee who made this work possible. Thank you for your constant guidance, mentoring, patience, motivation and time. I am blessed to be your advisee and student because of the many learnings you imparted during the course of my study.

I would also like to acknowledge my thesis committee, Professor Dr. Sanong Ekgasit, Associate Professor Dr. Apichat Imyim, and Dr. Tewarak Parnklang, Thank you for your kind suggestions and support.

To the Chulalongkorn University Office of Academic Affairs and the Department of Chemistry, it is an honor to receive the Graduate Scholarship for ASEAN or Non-ASEAN countries. I am forever grateful for this opportunity.

To Philippine Textile Research Institute's former Director Celia Elumba, former TSD Chief May Rico, my former Supervisor Lolit Palacol, and friends, Donna, Shyne and Marilou, thank you for allowing me to take this journey. I truly appreciate your support.

To my fellow Filipino Chula students who have been the source of strength and motivation, thank you. To my laboratory mates, thank you for always showing your support. I wish you all good luck in your future endeavors.

And to my family, especially my mother, this is all for you.

Charles Oliver Avenido

## TABLE OF CONTENTS

	Page
.....	iii
ABSTRACT (THAI).....	iii
.....	iv
ABSTRACT (ENGLISH).....	iv
ACKNOWLEDGEMENTS.....	v
TABLE OF CONTENTS.....	vi
LIST OF TABLES.....	x
LIST OF FIGURES.....	xi
1. Chapter I INTRODUCTION.....	1
1.1 Statement of Background and Problem.....	1
1.2 Research Objectives.....	5
1.3 Scope of Research.....	6
1.4 The benefit of this research.....	6
2. Chapter II Theory and Literature Review.....	7
2.1 Localized Surface Plasmon Resonance (LSPR).....	7
2.2 Silver Nanoparticles (AgNPs).....	10
2.2.1 Synthesis of Silver Nanoparticles.....	11
2.2.2 Synthesis of Silver Nanoprisms (AgNPrs).....	13
2.2.3 Colorimetric sensing using AgNPs.....	15
2.2.4 Dual-shaped silver nanoparticles.....	17
2.2.5 Silver nanoparticles (AgNPs) for hydrogen peroxide detection.....	18

2.3 Ratiometric Measurement .....	22
3. Chapter III Experimental .....	23
3.1 Materials and Chemicals.....	23
3.2 Instruments and Equipment .....	23
3.3 Preparation and Characterization of Silver Nanoparticles (AgNPs).....	24
3.3.1 Preparation of 2% starch solution.....	24
3.3.2 Synthesis of silver nanosphere (AgNSs).....	24
3.3.3 Synthesis of silver nanoprisms (AgNPrs).....	25
3.4 Characterization of AgNPs.....	26
3.5 Detection of Hydrogen Peroxide Using a Dual-Shaped Plasmonic Silver Nano-Sensor.....	26
3.5.1 Preliminary studies using concentrated hydrogen peroxide.....	26
3.5.2 Effect of Silver Nanoprism Seeds .....	27
3.5.3 Effect of AgNSs:NPrs ratio .....	27
3.5.4 Effect of the Volume of Concentrated Hydrogen Peroxide.....	28
3.6 Optimization of the sensor for the diluted H <sub>2</sub> O <sub>2</sub> detection.....	29
3.6.1 Effect of AgNSs/NPrs ratio .....	29
3.6.2 Effect of AgNSs/NPrs concentration .....	30
3.7 Analytical Performance .....	30
3.7.1 Response time.....	31
3.7.2 Selectivity Test .....	32
3.7.3 Accuracy and Precision.....	32
3.7.4 Application to real samples.....	34
4. Chapter IV Results and Discussion .....	35



4.1 Preparation of Silver Nanospheres (AgNSs).....	35
4.2 Preparation of Silver Nanoprisms (AgNPrs).....	35
4.3 Characterization of Silver Nanoparticles.....	38
4.4 Detection of Hydrogen Peroxide Using a Dual-Shaped Plasmonic Silver Nano-Sensor.....	40
4.4.1 Preliminary studies using concentrated hydrogen peroxide.....	40
4.4.2 Effect of Silver Nanoprism Seeds .....	43
4.4.3 Effects of AgNSs to AgNPrs ratio and concentration.....	44
4.4.4 Effect of Volume of Concentrated Hydrogen Peroxide .....	46
4.5 Optimization of the Sensor for the Diluted H <sub>2</sub> O <sub>2</sub> Detection.....	50
4.5.1 Effect of AgNSs/NPrs ratio .....	50
4.5.2 AgNSs/NPrs concentration.....	52
4.6 Analytical Performance .....	54
4.6.1 Analytical figures of merit .....	54
4.6.2 Response time.....	57
4.6.3 Selectivity Test .....	58
4.6.3.1 Effect of common anions .....	58
4.6.3.2 Tolerance test for halides.....	61
4.6.4 Accuracy and Precision .....	63
4.6.5 Application to real samples.....	63
5. Chapter V Conclusion .....	65
Future Work .....	67
REFERENCES .....	69
VITA.....	80



จุฬาลงกรณ์มหาวิทยาลัย  
**CHULALONGKORN UNIVERSITY**

## LIST OF TABLES

	Page
Table 3.1 Summary of the AgNSs (400 ppm) volumes used to create different sensor ratios.....	28
Table 3.2 Summary of AgNPrs and AgNSs volume and concentrations that were mixed to make the sensor with 10 and 15 ppm AgNPrs concentrations. ....	29
Table 3.3 Summary of AgNSs and AgNPrs volume and concentration mixed for 2:1 ratio sensors with different concentrations.....	30
Table 3.4 Summary of the AgNSs and AgNPrs volume and concentration to make the different 2:1 AgNSs/NPrs concentration for the analytical performance evaluation....	31
Table 3.5 Summary of the volume and concentration of the AgNSs/NPrs sensor, hydrogen peroxide and ultrapure water used for the accuracy and precision testing. ....	33
Table 4.1. Digital images of the diluted dual-shaped silver nanoparticle sensor and lone silver nanospheres after reacting with concentrated H <sub>2</sub> O <sub>2</sub> . ....	44
Table 4.2 Digital images of sensors with varying AgNSs:NPrs ratios before and after treatment of 9.79 mM hydrogen peroxide (50 $\mu$ L). ....	52
Table 4.3 Digital images of sensors with different concentrations at 2:1 AgNSs:NPrs ratio before and after treatment of 9.79 mM hydrogen peroxide (50 $\mu$ L). ....	53
Table 4.4 The analytical figures of merit obtained from different 2:1 AgNSs:NPrs concentrations.....	56
Table 4.5 Accuracy and precision of the AgNSs/NPrs sensor expressed as %recovery and %relative standard deviation (RSD). ....	63
Table 4.6 Accuracy and precision of the sensor for analysis of hydrogen peroxide in drinking water samples.....	64

## LIST OF FIGURES

	Page
Figure 2.1 Schematic comparison of a) propagating surface plasmon resonance (SPR) and b) Localized SPR. <sup>34</sup> .....	8
Figure 2.2 Representative electron microscopy images of synthesized AgNPs: a) silver nanosphere, b) silver necklaces, c) silver nanobars, d) silver nanocubes, e) silver nanoprisms, f) silver bipyramids, g) silver nanostars, h) silver nanowires, i) silver nanoparticles embedded silica particles. <sup>41</sup> .....	10
Figure 2.3 Silver nanosphere synthesis by chemical reduction with NaBH <sub>4</sub> . <sup>56</sup> .....	13
Figure 2.4 2D structure depiction of trisodium citrate. <sup>63</sup> .....	14
Figure 2.5 Schematic illustration of the formation of the metalloimmunoassay using both the s-AgNP-Ab and AgNC-Ab bioconjugates in the presence of the biomarker. <sup>33</sup> .....	18
Figure 3.1 Digital images of the red citrate-capped AgNPrs throughout the centrifugation process.....	25
Figure 4.1 Schematic diagram of the synthesis of silver nanoprisms.....	36
Figure 4.2 a) Extinction spectra of AgNSs (20 ppm) and AgNPrs (20 ppm) (inset: images of yellow AgNSs and red AgNPrs), b) TEM micrograph of mixed AgNSs/NPrs sensor c) and size distribution histogram of (i) AgNSs and (ii) AgNPrs.....	39
Figure 4.3 a) Schematic diagram of the growth-based sensing of hydrogen peroxide using dual-shaped silver nanoparticles. b) Extinction spectra and TEM micrographs of the sensor c) before and d) after addition of concentrated hydrogen peroxide. ....	41
Figure 4.4 The extinction spectra of AgNSs, AgNPrs, AgNSs/NPrs sensor before and after addition of hydrogen peroxide and their individual colors when diluted and (inset) comparison of IPDPR $\lambda_{max}$ and IPDPR absorbance intensity of the silver nanoprisms and the sensor after addition of 2.5 $\mu$ L of concentrated hydrogen peroxide.....	42

Figure 4.5 Extinction spectra of the AgNPrs and AgNSs/NPrs sensor with varying silver nanospheres concentration after addition of concentrated hydrogen peroxide. Inset: images of diluted AgNPrs and treated AgNSs/NPrs sensors.....	45
Figure 4.6 Effect of the volume of concentrated hydrogen peroxide to the a) IPDPR $\lambda_{\max}$ and absorbance intensities with respect to the AgNPrs $\lambda_{\max}$ and b) colors generated by the treated sensor after dilution. Inset: shape transformation of AgNPrs. ....	47
Figure 4.7 a) Extinction spectra of the sensor treated with different volumes of concentrated hydrogen peroxide. b) A calibration plot of H <sub>2</sub> O <sub>2</sub> concentration against the ratio of IPDPR and DPR. c) Digital images of color transition generated in this linear range. ....	49
Figure 4.8 A plot of the change in DPR and IPDPR absorbance after addition of 50 $\mu$ L 9.79 mM hydrogen peroxide into different AgNSs:NPrs sensor ratio. ....	51
Figure 4.9 Extinction spectra of 2:1 AgNSs/NPrs sensor ratio with different concentrations (ppm) after treatment of 9.79 mM of hydrogen peroxide.....	53
Figure 4.10 Plots of the linear ranges of the a) 20:10 ppm and b) 80:40 ppm AgNSs/NPrs sensors. ....	56
Figure 4.11 Digital images of the 80:40 ppm AgNSs/NPrs sensor after treatment with increasing hydrogen peroxide concentration.....	57
Figure 4.12 Effect of the response time on the IPDPR $\lambda_{\max}$ and absorbance intensity after addition of H <sub>2</sub> O <sub>2</sub> . ....	58
Figure 4.13 a) Extinction spectra, b) change in absorbance, and c) digital images of the 20:10 sensor before (blank) and after addition of the anions and H <sub>2</sub> O <sub>2</sub> . ....	60
Figure 4.14 Plots of the DPR, IPDPR and IPDPR/DPR shift after addition of a) iodide, b) bromide, and c) chloride for tolerance study. ....	62

## Chapter I INTRODUCTION

### 1.1 Statement of Background and Problem

Hydrogen peroxide ( $H_2O_2$ ) is a colorless and slightly pungent liquid that is made up of a single oxygen-oxygen bond. It has disinfectant, antiviral, and antibacterial properties due to its oxidizing power.<sup>1</sup> It is extensively employed as a cleaning or bleaching agent in household, pulp and paper, electronics and nuclear industries, and a key raw material for the chemical and pharmaceutical industries.<sup>2</sup>

In biological systems, it is a product of aerobic metabolism that is vital in signal transduction and regulation of biological processes, namely killing of invading pathogens, growth, and survival.<sup>3-5</sup> Hydrogen peroxide's role as a reactive oxygen species (ROS) is essential in maintaining the physiological balance in living systems. However, abnormal release or  $H_2O_2$  buildup causes severe damage of proteins and DNA that contributes to serious human diseases including auto-immune diseases, cancer, diabetes, neurodegenerative Alzheimer's, Parkinson's, and Huntington's diseases.<sup>6,7</sup> Oxidase enzymes are also responsible for the production of  $H_2O_2$  from a wide range of biological substrates that can reveal health conditions such as glucose or cholesterol. Through enzyme-linked immunoassay (ELISA),  $H_2O_2$ -generating enzymes could also be utilized to determine cancer biomarkers.<sup>8</sup> Hence, the development of hydrogen peroxide detection techniques has been the focus of numerous research in recent years.

To quantify hydrogen peroxide, several analytical methods have been developed, namely titrimetry<sup>9</sup>, spectrophotometry<sup>10</sup>, luminescence<sup>11</sup>, and electrochemistry<sup>12</sup>. Titrimetry, chemiluminescence, and spectrophotometric techniques are not convenient for routine and high-throughput analysis because of low selectivity and resolution, long detection time, and complicated instrumentation.<sup>13</sup> Optical methods, such as colorimetry, can serve as a reliable substitute for the aforementioned techniques because they are simple, instrument-free and able to attain ultra-low sensitivity.<sup>14</sup>

Colorimetric sensing of hydrogen peroxide typically uses horseradish peroxidase (HRP) and chromogenic dyes, such as 3,3',5,5'-tetramethylbenzidine (TMB), 3,3'-diaminobenzidine (DAB) or ortho-phenylenediamine (OPD) that change color when oxidized with H<sub>2</sub>O<sub>2</sub>.<sup>15, 16</sup> Natural enzymes like HRP are expensive and require specific conditions in which if not maintained can lead to permanent loss of enzymatic activity. To minimize errors and facilitate routine analysis, it is important to develop new techniques or materials that no longer utilize enzymes. Artificial enzymes called nanozymes which have peroxidase-like activity, appear to be a potent alternative by addressing the above-mentioned drawbacks. Although nanozymes are promising alternative to enzymes, they still require dyes and have limited selectivity, ambiguous mechanisms, and potential toxicity.<sup>15</sup>

Aside from enzyme-mimicking properties, nanoparticles such as gold and silver can be etched or enlarged as a sensing strategy. Several research described the decomposition or sculpturing of silver nanospheres, nanoplates or nanoprisms to detect different analytes such as halides,<sup>17, 18</sup> nickel,<sup>19</sup> mercury,<sup>20</sup> chromate,<sup>21</sup> hypochlorite,<sup>22</sup> and catecholamines.<sup>23</sup> Clearly, silver nanoparticles can be oxidized by many substances and thus this technique is problematic when it comes to selectivity. Additionally, the etching strategy using single-colored solutions that fade as the concentration of analytes increases makes it difficult to be detected by naked-eyes. Monochromic color change has limited the sensitivity and selectivity for visual detection. A diverse color change is crucial to improve the accuracy of detection.<sup>24</sup>

Growth-based plasmonic sensing is typically employed for enzyme-linked immunosorbent assay or ELISA. Hydrogen peroxide can induce the growth of gold nanoparticles (AuNPs) enabling the ultralow ( $1 \times 10^{-18}$  M) measurement of prostate-specific antigen and HIV.<sup>25</sup> Silver ions can also be reduced into  $\text{Ag}^0$  by ascorbic acid that can deposit onto AuNPs to detect antigens (IgG).<sup>26</sup> The enlargement of the nanoparticles and absorbance amplification is linear to the logarithm of IgG concentration from  $7 \times 10^{-13}$  to  $7 \times 10^{-11}$  M.

Evidently, ultrasensitive detection is made possible with enlargement of gold nanoparticles; however, the colors generated from these research are still limited to one or two colors.<sup>27</sup> Gold nanoparticles are more stable than silver



nanoparticles (AgNPs) because of their resistance to oxidation, however, they are more costly. AgNPs are sensitive to oxidation by many substances, but a variety of stabilizers can inhibit this problem. Silver nanoprisms (AgNPrs) remain highly sensitive despite the presence of stabilizers owing to its sharp tips and edges that can enhance electromagnetic field interaction. This leads to a sharper or more prominent extinction band than that of AuNPs which is highly favorable for sensing.<sup>28</sup> In recent years, AgNPs have enabled label-free or enzyme-free detection, which does not require chromogenic dyes and HRP, reducing the cost and use of reagents while providing a simple and quick method of detection.

Previously, silver nanoprisms with different morphology and colors ranging from yellow, orange, red, purple, to blue were created by treating starch-stabilized silver nanospheres (AgNSs) with varying amounts of hydrogen peroxide.<sup>29</sup> Hydrogen peroxide is known to sculpt silver nanospheres into nanoprisms or nanoplates.<sup>30-32</sup> Moreover,  $H_2O_2$  can oxidize silver nanospheres and simultaneously reduce the generated silver ions to silver metal. This unique bimodal redox mechanism creates an opportunity for highly selective colorimetric sensing of hydrogen peroxide which has not been achieved with previous decomposition-based silver nanoparticle sensors.<sup>27</sup>

In this work, a simple, highly sensitive and selective plasmonic silver nanoparticle sensor consisting of yellow starch-stabilized silver nanospheres (AgNSs)

and red citrate-capped silver nanoprisms (AgNPrs) will be developed for highly selective detection of hydrogen peroxide that can enable colorimetric detection owing to the ability of silver nanoprisms to produce multiple colors that are dependent on their geometry and size. Recently, mixing of two nanoparticle shapes was done to expand the linearity and sensitivity of electrochemical detection of a biomarker.<sup>33</sup> This dual-shaped plasmonic sensor (AgNSs/NPrs) leverages on (1) the unique ability of hydrogen peroxide to oxidize AgNSs and regenerate the released Ag<sup>+</sup> into silver metal, and (2) the selective attachment of citrate molecules on the surface of the AgNPrs which would ensure anisotropic growth will be maintained along the lateral sides of the nanoprism. Hydrogen peroxide-induced growth of silver ions onto silver nanoparticles and the use of dual-shaped silver nanoparticles have not been reported for colorimetric sensing purposes as of this writing.<sup>33</sup> We hypothesized that this enzyme-free sensor through its unique reaction with hydrogen peroxide would yield distinct colors that would result in a more selective and sensitive compared to etching-based plasmonic sensors.

## 1.2 Research Objectives

To develop a plasmonic sensor using a dual-particle silver nanosphere and silver nanoprism system for the enzyme-free detection of hydrogen peroxide.

### 1.3 Scope of Research

This study focused on the synthesis, characterization, and optimization of an AgNSs/NPrs sensor. UV-Vis Spectrophotometry and TEM imaging analysis were employed to confirm the size and morphology of the nanoparticles. The sensor's selectivity was tested against common anions. Its analytical performance was validated by measuring hydrogen peroxide in water samples. Analytical performance such as selectivity, linear range, detection limit, limit of quantitation, accuracy and precision of the developed hydrogen peroxide sensor was evaluated.

### 1.4 The benefit of this research

A dual-shaped silver plasmonic sensor (AgNSs/NPrs) for the detection of hydrogen peroxide was obtained. Growth-based sensing using dual-shaped silver nanoparticles is a potential alternative for hydrogen peroxide determination as it enables a highly selective and sensitive colorimetric and naked-eyes approach with high accuracy and precision.

## Chapter II Theory and Literature Review

### 2.1 Localized Surface Plasmon Resonance (LSPR)

Light can be confined in metal surfaces that are smaller than its wavelength when surface electrons oscillate in harmony with the incident radiation frequency. This results in an intense extinction band in the visible region that gives rise to a variety of colors. This phenomenon is called localized surface plasmon resonance or LSPR.<sup>34</sup> Metals such as gold, silver or copper have a filled d-band and a partially filled s-band (hybridized with p-band). These electrons in the partially filled bands participate in the oscillation process.<sup>28</sup> Coinage metals silver (Ag), gold (Au) and copper (Cu) nanoparticles (NPs) are more relevant than other transition metals because they can absorb strongly in the visible and near infrared region as a result of greater excitation of electric field on their surfaces.<sup>35</sup>

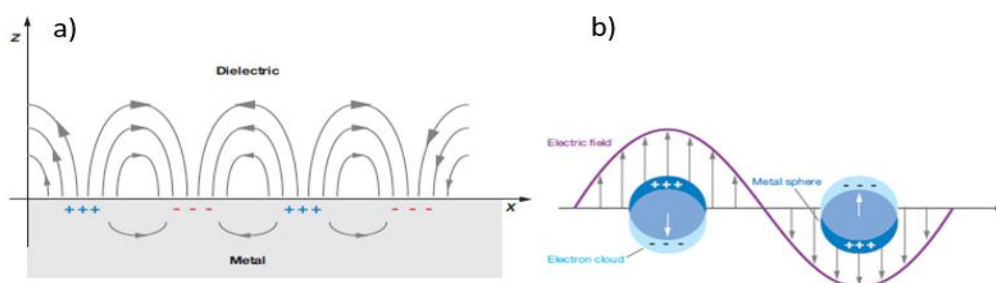
The Mie theory<sup>36</sup> is a useful classical model that can explain these brilliant properties which can also estimate the absorption spectrum of a metal sphere:

$$E(\lambda) = \frac{24\pi^2 N a^3 \epsilon_{\text{out}}^{3/2}}{\lambda \ln(10)} \left[ \frac{\epsilon_i}{(\epsilon_r(\lambda) + 2\epsilon_m)^2 + \epsilon_i(\lambda)^2} \right] \quad (2.1)$$

**Equation 2.1** states that the extinction spectrum  $E(\lambda)$  (elastic light-scattering plus absorption spectrum), is dependent on  $\epsilon_i$  and  $\epsilon_r$  (imaginary and real components of dielectric function of the metal, respectively),  $\epsilon_{\text{out}}$  which is the dielectric constant of the external environment, and radius  $a$  of a spherical

nanoparticle.<sup>35,36</sup> Yet, there is a limitation to this theory. It is only applicable to monodispersed spherical nanoparticles and surrounding medias. Additionally, the dipole approximation fails when radius is more than 20 nm. It does not consider matrix effects and cannot work on other geometries such as rods, stars, or prisms.

Gans introduced the concept of aspect ratio to modify the Mie theory. Aspect ratio is the ratio of major axis length to the minor axis length. The energy gap between resonance frequencies of two plasmonic bands increases as the aspect ratio increases which is important for refractive index technique. The Mie-Gans theory says that the LSPR of metallic nanoparticles is associated with its size, shape, composition, interparticle distance, and dielectric constant.<sup>37</sup> However, this still cannot consider the stronger interparticle coupling than the coupling with the surrounding since it only factors in dilute matrices or distant particles. To resolve this, Maxwell Garnett developed the effective medium theory which is valid for close particle systems.<sup>35</sup>



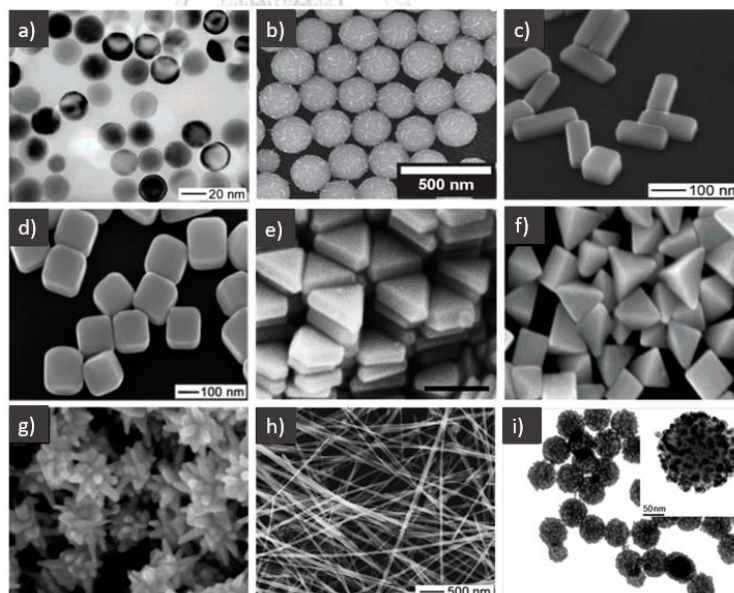
**Figure 2.1** Schematic comparison of a) propagating surface plasmon resonance (SPR) and b) Localized SPR.<sup>34</sup>

**Figure 2.1** illustrates the difference between **a)** propagation and decay of plasmons in two dimensions and its **b)** oscillation in LSPR. For SPR, electrons on the surface of the metal are displaced by the electromagnetic and an opposing charge develops on the other side of the surface. This charge separation follows, and a linear restoring force is experienced through positive nuclei's pulling effect. In contrast, LSPR shows polarization of the electron cloud upon electromagnetic stimulation. The electromagnetic radiation wavelength is larger than the diameter of the nanoparticles that it interacts with resulting in a plasmon that oscillates around the nanoparticles.<sup>34, 35, 38</sup>

Silver nanoprisms, nanoplates or nanodisks are two-dimensional nanomaterials that have extreme degree of anisotropy due to its much longer lateral side compared to its thickness. This structure makes its local surface plasmon resonance highly tunable and thus maximizing its electromagnetic field.<sup>31</sup> The LSPR wavelength is sensitive to truncation or rounding of tips of nanoprisms. Hence, etching of the nanoprisms has been a common approach for sensing. Electromagnetic coupling between nearby nanoparticles is another factor that determines the LSPR wavelength. Thus, analyte-induced aggregation/disaggregation can be yet another mechanism for sensing.<sup>28</sup> In this work, the LSPR wavelength change is due to the growth of the silver nanoprisms.

## 2.2 Silver Nanoparticles (AgNPs)

In 1889, M.C. Lea first reported the synthesis of citrate-stabilized silver nanoparticles with diameters ranging from seven to nine nanometers.<sup>39</sup> As early as 1897, a nanosilver formulation has been manufactured commercially for medical purposes.<sup>40</sup> Aside from its extensive biomedical use<sup>41</sup>, innovation in silver nanotechnology has been wide-spread in agriculture, electronics, robotics and food and textile industries. AgNPs' versatility stem from its unique characteristics specifically, excellent electrical and thermal conductivity, and brilliance.<sup>42</sup> **Figure 2.2** shows representative geometries of silver that can be obtained by controlling the synthesis chemistry.<sup>41</sup>



**Figure 2.2** Representative electron microscopy images of synthesized AgNPs: a) silver nanosphere, b) silver necklaces, c) silver nanobars, d) silver nanocubes, e) silver nanoprisms, f) silver bipyramids, g) silver nanostars, h) silver nanowires, i) silver nanoparticles embedded silica particles.<sup>41</sup>

### 2.2.1 Synthesis of Silver Nanoparticles

AgNPs can be prepared via three general synthesis routes, namely chemical, physical, and biological methods.<sup>43</sup> The two main approaches to synthesize AgNPs are bottom-up and top-down methods.<sup>28, 42</sup>

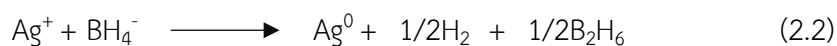
Top-down methods involve the breakdown of bulk metal to nano-sized materials via physical or mechanical means such as laser ablation, thermal decomposition, grinding, milling, and etching. Tsuji et al. (2002)<sup>44</sup> synthesized AgNPs by laser beam irradiation with different wavelengths. As the wavelength decreases, AgNPs are formed. Navaladian and team (2006)<sup>45</sup> prepared AgNPs from the thermal decomposition of silver oxalate in the presence of polyvinyl alcohol (PVA) as a capping agent in ethylene glycol. Silver oxalate can decompose to silver metal and carbon dioxide at around 140 °C. The major downside of these top-down methods is the development of defects on the surface of Ag nanostructures that give rise to undesirable effects to their physicochemical properties. Furthermore, the process is slow and requires enormous amount of energy.<sup>42, 46</sup>

The bottom-up approach, on the other hand, pertains to the enlargement of atomic particles or clusters into bigger nanostructures through self-assembly, step-wise, or one-pot procedure. Surface imperfections are minimized with this approach and excellent uniformity of size and morphologies are achieved. Bottom up fabrication of silver nanoparticles can be done through chemical

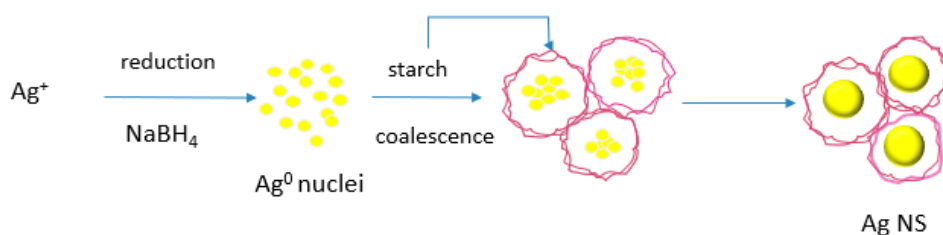


reduction<sup>32, 47, 48</sup>, photoinduced aggregation<sup>49</sup>, vapor deposition<sup>50</sup>, polyol reduction<sup>51</sup>, electrochemical,<sup>52</sup> and biological approach like green synthesis<sup>53</sup> using microorganisms or plant extracts.<sup>42, 54</sup> Among these methods, the chemical reduction method is widely used because of its efficiency, high productivity and minimal cost.

For chemical reduction methods, the growth and shape of the silver nanostructures are controlled by three essential elements: (1) precursor silver salt, (2) reducing agents, and (3) capping or stabilizing agents. Silver nitrate is the most common silver salt that can be reduced by various reducing agents, specifically sodium citrate, sodium borohydride, ascorbic acid, alcohols, hydrazines, hydroquinone, glucose, and N,N-dimethylformamide (DMF). Stabilizing agents that have reducing capability and can protect AgNPs from aggregation and oxidation include polysaccharides, surfactants, ligands, or polymers. Sodium borohydride (NaBH<sub>4</sub>) one of the strongest reducing agents, can produce small silver nanoparticles.<sup>42, 46, 55</sup> The reaction of silver and NaBH<sub>4</sub> is as follows:



**Figure 2.3** shows how silver nanoparticles are formed by reduction of silver nitrate with sodium borohydride as a reducing agent and starch as a stabilizer. Reduced silver initially forms nuclei that coalesce into nano clusters and finally assembles into silver nanospheres (AgNSs).



**Figure 2.3** Silver nanosphere synthesis by chemical reduction with  $\text{NaBH}_4$ .<sup>56</sup>

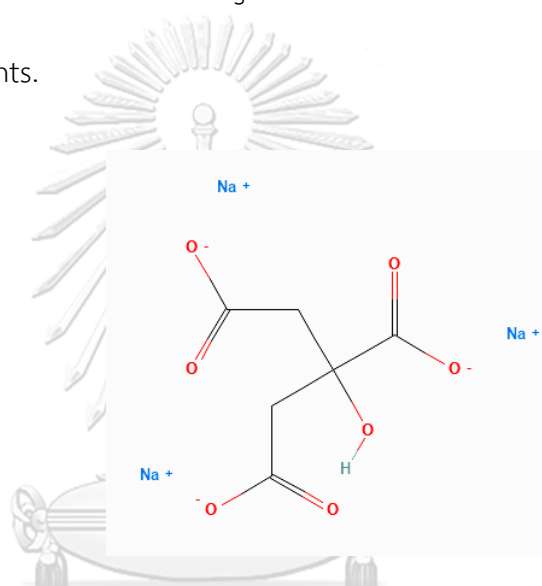
### 2.2.2 Synthesis of Silver Nanoprisms (AgNPrs)

Métraux and Mirkin (2005)<sup>57</sup> reported a chemical protocol that offers AgNPrs with unimodal size distribution. Silver nitrate was reduced by  $\text{NaBH}_4$ , in conjunction with trisodium citrate, poly(vinylpyrrolidone) and hydrogen peroxide. Increase of  $\text{NaBH}_4$  concentration results in a decrease in thickness while the edge length increases modestly.<sup>28</sup> Without citrate, they found out that nanoprisms cannot be formed. Through a systematic study of Zhang et al. (2011), hydrogen peroxide was found to be the key ingredient to the formation of AgNPrs instead of citrate.

Silver nanoprisms can also be synthesized by a seed-mediated approach.

Aherne and colleagues (2008)<sup>58</sup> prepared silver nanoprisms through a two-step process, in which silver nanoparticle seeds were first prepared by borohydride reduction in the presence of trisodium citrate and poly(sodium styrene sulphonate). This was followed by reduction of additional  $\text{AgNO}_3$  by ascorbic acid promoting the growth of AgNPrs. This protocol is a rapid and highly reproducible way to produce high quality silver nanoprisms.

Citrate, usually comes from trisodium citrate (**Figure 2.4**) or citric acid and is widely used in the silver or gold nanoparticle synthesis.<sup>31, 59-62</sup> Jiang et al. (2010)<sup>59</sup> revealed that citrate has multiple roles in the synthesis of silver nanoplates. They found out that citrate can be a reducing agent, a stabilizer, and a complexing agent. Trisodium citrate's reducing power is much weaker compared to that of sodium borohydride or ascorbic acid. Its stabilizing effect is much weaker than the surfactants tested in the experiments.



**Figure 2.4** 2D structure depiction of trisodium citrate.<sup>63</sup>

Kilin et al. (2008)<sup>64</sup> found out in their *ab initio* study that four Ag-O bonds can form due to the matching of the three-fold symmetry of citrate and Ag(111). At Ag(100), citrate forms only two connections because of the geometry disparity. A hydrogen atom of the citric acid also migrates which triggers the electrons of the carboxyl oxygen atom and results in enhanced binding affinity toward the Ag(111) plane. The preferential binding energy of citric acid to Ag(111) promotes crystal

growth along the Ag(100) surface hence, controlling the shape of the silver nanoparticles.<sup>64</sup>

Zhang and group (2010)<sup>30</sup> demonstrated that lateral growth of silver nanoplates can be accomplished by combining the concept of seeded growth and selective ligand adhesion. Ag-citrate was used as precursors for this work. Citrate ligand blocks the (111) facet of the silver nanoplates to ensure that addition of silver only occurs at the lateral direction. High aspect ratio due to the narrow thickness of the plate was achieved making the surface plasmon resonance band narrow which is favorable for practical applications.

### 2.2.3 Colorimetric sensing using AgNPs

Aggregation and non-aggregation-based sensing are strategies for colorimetric sensing using metal nanoparticles. In an aggregation-based approach, the color generation is brought about by strong plasmonic coupling of neighboring nanoparticles, typically, gold or silver. Since the change in distance, shape or particle size strongly impacts the LSPR, any variation would cause a plasmon band shift that leads to a color change.<sup>24, 27</sup> Elghanian et al. (1997)<sup>65</sup> demonstrated that aggregation of mercaptoalkyloligonucleotide-modified Au nanoparticles changes the color of the solution from purple to red in the presence of target nucleotide stand.

One of the advantages of non-aggregation-based sensing is that it has no influence on the auto-aggregation of nanoparticles, therefore preventing false

positives or negative results. The non-aggregation approach can be classified as either an etching-based or growth-based methods.

Oxidative etching or decomposition of nanoparticles reduces their plasmon band intensity and causes a blueshift of the spectra.<sup>24, 27</sup> Silver nanoprism or nanosphere decomposition is widely used for sensing organic<sup>66</sup>, inorganic<sup>19, 20</sup> and biological<sup>67, 68</sup> analytes, which indicates a clear problem in selectivity. Furthermore, the etching-based AgNPs sensor only produces mono-color change that limits its naked eye application since human eyes are more sensitive to color changes than intensity changes.<sup>24, 69, 70</sup>

Growth-based sensing involves an increase in size of a nanoparticle seed due to the presence of a reducing target analyte and excess metal precursors (seed-mediated) or *in situ* formation of metal nanostructures from existing metal precursors (seed-free).<sup>27</sup> The growth of nanoparticles causes a shift in LSPR that can generate increase in color intensity or multi-color readout. This is important because accuracy of colorimetric detection using the naked eyes can be enhanced significantly with substrates that can produce a variety of colors.<sup>24</sup>

De la Rica and Stevens (2012)<sup>25</sup> demonstrated that hydrogen peroxide can induce the growth of gold nanoparticles (AuNPs) enabling the ultralow ( $1 \times 10^{-18}$  M) measurement of prostate-specific antigen and HIV. Between 120 and 100  $\mu$ M of hydrogen peroxide, the localized surface plasmon resonance peak redshifts, changing

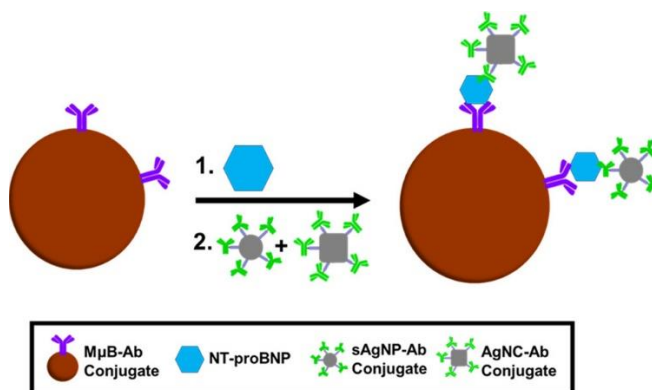
the color from red to blue. This low concentration of  $\text{H}_2\text{O}_2$  promotes the growth of gold ions onto the gold nanoparticles.

In 2018, Pham and team<sup>26</sup> grew silver ions onto AuNP-assembled silica to detect model analyte rabbit IgG (antigen). In the presence of the antigen, alkaline phosphatase, conjugated to a secondary antibody, catalyzes the conversion of 2-phosphoro-L-ascorbic acid to ascorbic acid that can reduce silver ions. The silver metal then deposits onto the AuNPs causing the enlargement of the nanoparticles and absorbance amplification that is linear to the logarithm of IgG concentration from  $7 \times 10^{-13}$  to  $7 \times 10^{-11}$  M.

#### 2.2.4 Dual-shaped silver nanoparticles

The use of dual-shaped nanoparticles as a biosensor was first reported by Pollok and team (2021)<sup>33</sup>. By combining the silver nanospheres (AgNSs) and silver nanocubes (AgNCs), a three-fold decrease in detection limit (LOD) of model immunoassay, 20% increase in collected charge, and decreased LOD of the NT-proBNP down to clinically relevant dynamic range were achieved via electrochemical analysis. In their work, the ratios of AgNSs and AgNCs were optimized for the immunoassay of N-terminal prohormone brain natriuretic peptide (NT-proBNP), a heart-failure marker (**Figure 2.5**). Lone silver nanospheres' LOD is five-fold higher than the clinical range. Improvement of the analytical performance after addition of

silver nanocubes was attributed to the more efficient galvanic exchange process of AgNCs.



**Figure 2.5** Schematic illustration of the formation of the metalloimmunoassay using both the s-AgNP-Ab and AgNC-Ab bioconjugates in the presence of the biomarker.<sup>33</sup>

### 2.2.5 Silver nanoparticles (AgNPs) for hydrogen peroxide detection

Several sensors were developed based on the oxidative etching of silver nanoparticles to detect hydrogen peroxide directly and other molecules such as glucose indirectly. This technique, however, is limited by its single visible color change that may be difficult to determine with the naked eye and by how silver nanoparticles can get etched by other substances.

Endo et al. (2010)<sup>71</sup>, Filippo et al. (2011)<sup>69</sup> and Vasileva et. al (2011)<sup>70</sup> described the LSPR-based hydrogen peroxide quantitation using silver nanospheres capped with polyvinylpyrrolidone (PVP), poly(vinyl alcohol) (PVA), and starch respectively. Decomposition of silver nanospheres by hydrogen peroxide caused the decrease of the surface plasmon band at 400 nm causing yellow to colorless

transition of the sensors. Coating AgNPs with polymers protects them from aggregation and oxidation by atmospheric oxygen.<sup>72</sup>

Tran et al. (2020)<sup>73</sup> recently developed a label-free hydrogen peroxide and cholesterol biosensor using silver nanoparticles as the probe. Cholesterol oxidase enzyme oxidizes cholesterol into cholest-4-en-3-one and H<sub>2</sub>O<sub>2</sub>. A color change from yellow, pink to clear with increasing H<sub>2</sub>O<sub>2</sub> concentration was observed upon oxidation of silver nanoparticles to Ag<sup>+</sup>. This method achieved a LOD at 3.5 μM. For cholesterol detection, the calculated LOD is approximately 40 μM.

Zuo et al. (2020)<sup>74</sup> converted dissolved oxygen to hydrogen peroxide using glucose and glucose oxidase (GOD) in a microfluidic chamber. Hydrogen peroxide etched the silver nanoprisms (AgNPrs) to silver ions. This reaction was detected using a CCD camera to indirectly measure the dissolved oxygen concentration. A detection limit of 3.52 μg/L was achieved in a range of 0 to 16 mg/L using this method. The conversion and etching reactions are as follows:



Lertvachirapaiboon et al. (2019)<sup>75</sup> demonstrated the measurement of hydrogen peroxide in a microfluidic chip using a smartphone camera. Red silver nanoprisms were synthesized and reacted with H<sub>2</sub>O<sub>2</sub>. The disintegration of silver nanoprisms can be detected as a color intensity shift. Using ImageJ, green



chromaticity was extracted from the digital images of the microfluidic channels. A linear range of 10 to 300  $\mu\text{M}$  was observed. The developed method was used to measure the  $\text{H}_2\text{O}_2$  spiked in tap water and bottled water. Smartphones and microfluidics enable the quick and simple quantification of silver nanoprisms and hydrogen peroxide in production processes.

Artificial enzymes or nanozymes have attracted a great deal of interest in the past decade because of their ability to overcome limitations of natural enzymes, specifically low stability, high cost, and difficult maintenance of environmental conditions. In 2007, Iron (II, III) oxide ( $\text{Fe}_3\text{O}_4$ ) was first reported to have peroxidase-mimicking activity. A broad selection of enzyme-mimicking nanomaterials has been discovered from then on, such as peroxidases, oxidases, catalases, haloperoxidases and hydrolases. Nanozymes have similar catalytic activity to natural enzymes. Furthermore, they are tunable, highly stable, easy to mass produce and have multiple enzyme mimetic activity. However, they also have some downsides such as potential toxicity or poor biocompatibility, limited substrate selectivity, ambiguous mechanism and catalytic properties that highly depend on morphology, size, and composition.<sup>15, 76</sup>

Monitoring of intracellular  $\text{H}_2\text{O}_2$  in single living cells in situ is crucial for better understanding of cellular processes and heterogeneity of tumor cells. Wang et al. (2022)<sup>77</sup> demonstrated that  $\text{Fe}_3\text{O}_4@\text{Ag}$  NP-based strategy is highly selective for

H<sub>2</sub>O<sub>2</sub> that leads to sensitive H<sub>2</sub>O<sub>2</sub> detection in cells. Fe<sub>3</sub>O<sub>4</sub>@Ag NPs exhibited low toxicity and good biocompatibility. The label-free bifunctional Fe<sub>3</sub>O<sub>4</sub>@Ag NPs were then applied for the SERS imaging of single B16 cells to obtain both intracellular and extracellular concentrations of H<sub>2</sub>O<sub>2</sub>. Fe<sub>3</sub>O<sub>4</sub>@AgNPs have peroxidase-like activity that can oxidize TMB. SERS intensity of the oxidized TMB provided a good linear response and a wide range from 1 fM to 1 mM of hydrogen peroxide.

Karim et al. (2018)<sup>78</sup> reported a silver nanoparticle nanozyme embedded on a cotton fabric that can detect glucose in urine. AgNPs' peroxidase-like activity catalyzed the oxidation of TMB by the •OH radicals from the breakdown of glucose by glucose oxidase. The Ag@Fabric showed better catalytic activity than horseradish peroxidase. However, like natural enzymes, the catalytic activity of the Ag@Fabric nanozyme is strongly dependent on several factors such as, pH, temperature, and time. The linear range of the silver nanozyme sensor was found to be 0.1 to 2 mM. The Ag@Fabric nanozyme sensor was validated using urine samples from healthy and diabetic individuals. The advantage of the free-standing nanozyme is its potential reusability. The researchers were able to obtain satisfactory recovery rates of 94-104%.

To summarize, hydrogen peroxide determination with AgNPs was previously accomplished through decomposition-based sensing and nanozyme coupled with chromogenic dyes. Very low detection limits were obtained with these

methods, however, colorimetric detection with the naked eyes, a more practical approach, would be difficult with their single color intensity change. Also, selectivity issues are prevalent since AgNPs can be etched by many substances. This work focuses on the development of growth-based sensing of  $H_2O_2$  with AgNSs and AgNPs that can produce multi-color change facilitating sensitive detection with naked eyes. Furthermore, selectivity is ensured by the unique reaction of the dual-shaped silver sensor with hydrogen peroxide.

### 2.3 Ratiometric Measurement

Common problems encountered in molecular imaging using an absolute intensity-dependent signal from a single nanoprobe include nonspecific and misleading images which lead to false positives. These are caused by several experimental or physiological factors. One way to lessen the effect of the nonspecific background signals is to use a ratiometric approach as opposed to a single intensity readout. Ratiometric analysis is based on self-calibration of signal intensity via measurement of two or more analyte-stimulated signals, one of which is acting as a reference that can normalize the other signals. There are two modes for the fabrication of ratiometric probes. One technique is to add a reference signal that is insensitive to the presence of the target analyte; the other is to operate two analyte-reactive signal changes that enable ratiometric analysis.<sup>79</sup> In this work we apply the second mode where the spectroscopic absorbances from the degradation of silver nanospheres and growth of silver nanoprisms were utilized as ratiometric signals.

## Chapter III Experimental

### 3.1 Materials and Chemicals

1. 30% (w/w) hydrogen peroxide ( $\text{H}_2\text{O}_2$ ) (Analytical reagent (AR) grade, Merck)
2. Silver nitrate ( $\text{AgNO}_3$ ) (Analytical reagent (AR) grade, Merck)
3. Sodium borohydride ( $\text{NaBH}_4$ ) (Analytical reagent (AR) grade, Sigma-Aldrich)
4. Trisodium citrate ( $\text{Na}_3\text{C}_6\text{H}_5\text{O}_7$ , TSC) (Analytical reagent (AR) grade, Merck)
5. Soluble starch (Analytical reagent (AR) grade, Merck)
6. Ultrapure water (Milli-Q)

All chemicals were used as received. All glassware and magnetic stir bars were washed with liquid detergent and rinsed with ultrapure water prior to use.

### 3.2 Instruments and Equipment

1. Hotplate stirrer (IKA C-MAG HS10)
2. Analytical balance (Mettler-Toledo)
3. Syringe Pump (Harvard Apparatus PHD 2000)
4. Rectangular quartz cuvette 10 mm path length, 2.5 mL volume (Brand GMBH + CO KG)
5. UV-Vis Spectrophotometer (Agilent HP8453)

6. JEOL JEM-1400 Flash Electron Microscope with 120 kV acceleration voltage
7. Eppendorf micropipettes (2.5 to 1000  $\mu\text{L}$ )
8. Eppendorf microcentrifuge tubes (1.5 ml)
9. Microcentrifuge (Stuart SCF3)

### 3.3 Preparation and Characterization of Silver Nanoparticles (AgNPs)

#### 3.3.1 Preparation of 2% starch solution

Ultrapure water (100 mL) was boiled on a hotplate. Starch (4 g) was dissolved in 100 mL of MilliQ water in a separate beaker. After dissolution, this was added to the boiling water and mixed with a magnetic stirrer. After boiling for another 30 minutes, the solution was cooled down to room temperature and adjusted to a 200 mL final volume with MilliQ water.

#### 3.3.2 Synthesis of silver nanosphere (AgNSs)

Silver nanospheres were synthesized using a chemical reduction process. To make 400 ppm of silver nanospheres, 0.126 g of silver nitrate is mixed with the 100 mL starch solution. In a separate beaker, 0.042 g of  $\text{NaBH}_4$  is mixed with the remaining starch solution. The silver nitrate solution is then injected into the  $\text{NaBH}_4$  solution at a rate of  $2 \text{ mL s}^{-1}$  while stirring continuously. The color immediately changed from colorless to yellow and finally, dark brown, indicating the generation of silver nanospheres. This colloid was vigorously stirred for 30 minutes before heating gently for 1.5 hours.

### 3.3.3 Synthesis of silver nanoprisms (AgNPrs)

Silver nanospheres were transformed into silver nanoprisms by a redox reaction triggered by concentrated hydrogen peroxide. Hydrogen peroxide (94.5  $\mu\text{L}$ ) was injected with a micropipette into the 25 mL silver nanospheres solution and then stirred vigorously with a magnetic stirrer for 30 minutes. Silver to hydrogen peroxide 1:10 molar ratio produces a reddish brown nanoprism colloid.

### 3.3.4 Citrate-capping of silver nanoprism

Initially, Silver nanoprisms (400 ppm) were mixed with a trisodium citrate solution (1000 ppm). Ultrapure water was added to make a total solution volume of 1.5 mL per Eppendorf tube. This mixture was incubated for at least 3 hours before centrifugation (12000 rpm, 30 minutes). To remove free citrate molecules, the nanoparticle precipitate was washed twice using Milli-Q water and then resuspended in Milli-Q water. **Figure 3.1** shows the colors of the citrate-capped AgNPrs before and after centrifugation and washing. The color of this solution is pink when diluted.



**Figure 3.1** Digital images of the red citrate-capped AgNPrs throughout the centrifugation process.

### 3.4 Characterization of AgNPs

UV-Vis Spectroscopy (Agilent HP8453) was used to monitor the plasmon resonance bands that would verify the presence and growth of silver nanoparticles. TEM (JEOL JEM-1400 Flash Electron Microscope) imaging and ImageJ software were used to analyze the morphology and mean diameter of the AgNPs.

### 3.5 Detection of Hydrogen Peroxide Using a Dual-Shaped Plasmonic Silver Nano-Sensor

#### 3.5.1 Preliminary studies using concentrated hydrogen peroxide

Growth of the nanoprisms was first observed through a redshift using 2.5:1 (97.5:39 ppm) AgNSs/NPrs ratio and concentrated hydrogen peroxide in a 2.5 mL total volume. **Table 3.1** shows the volume and concentration of the AgNSs and AgNPrs needed to produce this AgNSs/NPrs sensor. Concentrated hydrogen peroxide (2.5  $\mu$ L) was then mixed with the silver nano-sensor by pipetting up and down until the color of the sensor is totally dark. The AgNSs/NPrs sensor was diluted five-fold by taking 400  $\mu$ L of the treated sensor and mixing it with ultrapure water to make a total volume of 2 mL. The diluted sensor was analyzed using UV-Vis spectrophotometry. Untreated AgNSs/NPrs sensor was also measured to compare the dipole plasmon resonance (DPR) band absorbance ( $\sim$ 403 nm) and in-plane dipole plasmon resonance (IPDPR,  $\sim$ 485 to 510 nm) before and after addition of concentrated hydrogen peroxide. The plasmon bands of 20 ppm AgNSs and AgNPrs were also measured. Images of the cuvettes after the dilution was captured using a

Samsung S21 smartphone at ambient lighting. Digital images' contrast was increased by 40% using MS PowerPoint to show the vivid colors as seen by the naked eyes.

### 3.5.2 Effect of Silver Nanoprism Seeds

To know how the AgNPrs seeds are important to the sensing mechanism, the AgNSs/NPrs sensor and lone AgNSs were reacted with different volumes of concentrated hydrogen peroxide. Three AgNSs/NPrs sensors with 2:1 ratio and a concentration of 98:39 ppm were prepared and reacted with 1, 4 and 10  $\mu\text{L}$  of hydrogen peroxide. AgNSs with concentrations of 98 and 196 ppm were prepared and reacted with the same volumes of concentrated  $\text{H}_2\text{O}_2$ . After five-fold dilution, the images of the sensors were taken.

### 3.5.3 Effect of AgNSs:NPrs ratio

Initially, the effect of AgNSs to AgNPrs ratio was investigated using AgNPrs baseline concentration of 39 ppm and varying AgNSs concentration from 19.5 to 97.5 ppm. AgNPrs solutions (65 ppm) were prepared in a microcentrifuge tube by mixing 400 ppm of the AgNPrs (244  $\mu\text{L}$ ) with 1000 ppm trisodium citrate (150  $\mu\text{L}$ ). The total volume was adjusted to 1.5 mL with MilliQ water. The extracted AgNPrs after centrifugation and washing were transferred to an amber bottle and shaken prior to mixing with different AgNSs volumes indicated in **Table 3.1**. The total volume of the sensor in the cuvette was adjusted to 2.5 mL using ultrapure water. Concentrated  $\text{H}_2\text{O}_2$  (9.79 M, 2.5  $\mu\text{L}$ ) was added to the dual-shaped nano-sensor, which immediately



turned black after mixing. Colored solutions were obtained after five-fold dilution of the sensor. The extinction spectra of the sensors were measured before and after the addition of hydrogen peroxide.

**Table 3.1** Summary of the AgNSs (400 ppm) volumes used to create different sensor ratios.

AgNSs:NPrs <sup>a</sup> Sensor ratio	AgNSs concentration (ppm)	AgNSs (400 ppm) volume (mL)	MilliQ water volume (mL)
0.5:1	19.5	0.113	0.760
1:1	39.0	0.225	0.648
2:1	78.0	0.450	0.423
2.5:1	97.5	0.563	0.310

<sup>a</sup>AgNPrs (65 ppm) volume is 1.5 mL.

#### 3.5.4 Effect of the Volume of Concentrated Hydrogen Peroxide

Using the 2:1 ratio of silver nanospheres to nanoprisms, the effect of varying hydrogen peroxide concentration to the sensor was studied by adding concentrated H<sub>2</sub>O<sub>2</sub> from 0.1 to 30  $\mu$ L to yield a final concentration of 0.39 mM to 117.5 mM. The AgNSs/NPrs sensor and hydrogen peroxide were mixed for 15 seconds by pipetting up and down until the colloid turns completely dark. The sensor was 5-fold diluted with ultrapure water prior to UV-Vis analysis.

A calibration curve was plotted using ratiometric absorbance data (IPDPR/DPR) of the sensors treated with 0.1 to 3  $\mu$ L hydrogen peroxide (final concentration: 0.39 to 19.6 mM) Linear range, Limit of Detection (LOD) and Limit of

Quantitation (LOD) were determined from this plot. Images of the diluted AgNSs/NPrs sensors were taken after dilution.

### 3.6 Optimization of the sensor for the diluted H<sub>2</sub>O<sub>2</sub> detection

#### 3.6.1 Effect of AgNSs/NPrs ratio

To eliminate the dilution step and further reduce the limit of detection, the concentration of silver nanoparticles was reduced. At this lower concentration level, optimal AgNSs:NPrs ratio was investigated by preparing 0.5:1 to 2:1 AgNSs:NPrs ratio as indicated in **Table 3.2**. The concentrations of AgNPrs used were 10 and 15 ppm. The total volume of the mixture was adjusted to 1.95 mL with MilliQ water. Hydrogen peroxide (9.79 mM, 50  $\mu$ L) was prepared and mixed with the sensors by pipetting up and down for 15 seconds. Absorbance values at the IPDPR and DPR  $\lambda_{\max}$  of the AgNSs and AgNPrs were obtained using UV-Vis spectroscopy.

**Table 3.2** Summary of AgNPrs and AgNSs volume and concentrations that were mixed to make the sensor with 10 and 15 ppm AgNPrs concentrations.

AgNPrs concentration (ppm)	AgNSs:NPrs ratio (concentration, ppm)	AgNPrs (80 ppm) volume (mL)	AgNSs (400 ppm) volume (mL)
10	0.5:1 (5:10 ppm)	0.25	0.025
	1:1 (10:10 ppm)	0.25	0.050
	1.5:1 (15:10 ppm)	0.25	0.075
	2:1 (20:10 ppm)	0.25	0.100
15	0.5:1 (7.5:15 ppm)	0.375	0.037
	1:1 (15:15 ppm)	0.375	0.075
	1.5:1 (22.5:15 ppm)	0.375	0.113
	2:1 (30:15 ppm)	0.375	0.150

### 3.6.2 Effect of AgNSs/NPrs concentration

Using the 2:1 AgNSs:AgNPrs ratio, concentrations 10:5, 15:7.5 and 20:10 ppm were treated with 9.79 mM of H<sub>2</sub>O<sub>2</sub> (50 µL) to compare the effect of the concentration on the color and spectra of the AgNSs/NPrs sensors. The AgNSs/NPrs sensor volume was adjusted to 1.95 mL using ultrapure water prior to addition of hydrogen peroxide. **Table 3.3** shows the volume of the AgNSs (400 ppm) and AgNPrs (80 ppm) that were added to make the sensors.

**Table 3.3** Summary of AgNSs and AgNPrs volume and concentration mixed for 2:1 ratio sensors with different concentrations.

AgNSs:AgNPrs Concentration (ppm)	Volume (mL) of 80 ppm AgNSs	Volume (mL) of 400 ppm AgNPrs	MilliQ water volume (mL)
10:5	0.050	0.125	1.775
15:7.5	0.075	0.188	1.687
20:10	0.100	0.250	1.600

### 3.7 Analytical Performance

AgNSs/NPrs sensor ratios and concentrations listed in **Table 3.4** were prepared using 400 ppm of AgNSs and 80 ppm of citrate-capped AgNPrs. Each sensor ratio was reacted to a range of hydrogen peroxide standard solutions within the range of 0.625 mM and 4000 mM. The final volume of the 20:10 ppm AgNSs/NPrs

was adjusted to 2 mL while the rest of the sensors were 2.5 mL. Calibration plots were built from the ratiometric data obtained from UV-Vis analysis of the treated sensors. Detection limit (LOD) was computed based on the  $3\sigma/\text{slope}$ , where  $\sigma$  was the standard deviation of blank samples and slope is obtained from the calibration curve while limit of quantitation (LOQ) is  $10\sigma/\text{slope}$ . The 20:10 sensor was no longer diluted prior to UV-vis analysis while the 40:20, 60:30 and 80:40 AgNSs/NPrs sensor ratios were diluted using a factor of 2.5, 3.33, and 5, respectively.

**Table 3.4** Summary of the AgNSs and AgNPrs volume and concentration to make the different 2:1 AgNSs/NPrs concentration for the analytical performance evaluation.

AgNSs:NPrs ratio (concentration, ppm)	Volume (mL) of 400 ppm AgNSs	Volume (mL) of 80 ppm AgNPrs	MilliQ water volume (mL)	Dilution factor for UV measurement
20:10	0.100	0.250	2.00	none
40:20	0.250	0.625	2.50	2.5
60:30	0.375	0.938	2.50	3.3
80:40	0.500	1.25	2.50	5.0

### 3.7.1 Response time

AgNSs/NPrs sensor ratio of 20:10 ppm was prepared. After the mixing of 50  $\mu\text{L}$  of 9.79 mM  $\text{H}_2\text{O}_2$  sample, the extinction spectra of the sensor were measured from 1 min to 30 min to obtain the optimum response time.

### 3.7.2 Selectivity Test

Common anions were evaluated against the selectivity of the silver nanoparticle sensor. Initially, one mM solutions were prepared and 50  $\mu$ L was mixed with the sensor. Extinction spectra were measured before and after addition of hydrogen peroxide to observe the change in intensity of the dipole plasmon resonance (DPR) and In-plane dipole plasmon resonance (IPDPR) bands. Change in the mean intensities at the extinction bands of the nanospheres and nanoprisms were calculated as follows:  $\Delta I = I_{\text{tested species}} - I_{\text{blank}}$  where blank is the AgNSs/NPrs sensor before incubating with different species.

### 3.7.3 Accuracy and Precision

The accuracy and precision of the developed AgNSs/NPrs sensor (78:39 ppm) was investigated using %recovery and %relative standard deviation of the measured hydrogen peroxide spiked in ultrapure water. A calibration curve was first created by measuring the absorbance at the DPR and IPDPR of the mixed AgNSs/NPrs sensor and standard samples with final concentration of hydrogen peroxide from 4 to 12 mM. The ratio of the IPPDR/DPR was plotted against the final concentration of hydrogen peroxide. The sensor was then reacted with the concentrated hydrogen peroxide to make the final concentrations of 5 and 10 mM hydrogen peroxide. **Table 3.5** summarizes the concentration and volume of the AgNSs, AgNPrs and hydrogen peroxide, and ultrapure water volume used in this experiment. Using the linear regression equation from the calibration curve, the concentrations of the spiked

samples were calculated. This experiment was done in two consecutive days (n=5).

% Recovery and %RSD were computed using **Equations 3.1 and 3.2.**

$$\% \text{ Recovery} = (C_1/C_2) \times 100\% \quad (3.1)$$

where  $C_1$  refers to the determined amount of  $H_2O_2$

$C_2$  refers to the known concentration of spiked  $H_2O_2$

$$\% \text{ RSD} = ( \sigma \times 100\% ) / \bar{x} \quad (3.2)$$

where  $\sigma$  refers to the standard deviation

$\bar{x}$  refers to the mean concentration of the analyte

**Table 3.5** Summary of the volume and concentration of the AgNSs/NPrs sensor, hydrogen peroxide and ultrapure water used for the accuracy and precision testing.

Solution	$H_2O_2$ conc. (mM)	Volume (mL)		Conc. $H_2O_2$	MilliQ vol.	Total
		400 ppm AgNSs	80 ppm AgNPrs			
$H_2O_2$ standards						
1	2	0.488	1.219	0.00051	0.792	2.5
2	4	0.488	1.219	0.00102	0.792	2.5
3	6	0.488	1.219	0.00153	0.791	2.5
4	8	0.488	1.219	0.00204	0.791	2.5
5	10	0.488	1.219	0.00255	0.790	2.5
6	12	0.488	1.219	0.00306	0.790	2.5
$H_2O_2$ samples						
1	5	0.488	1.219	0.00128	0.792	2.5
2	11	0.488	1.219	0.00281	0.790	2.5

### 3.7.4 Application to real samples

Two different brands of bottled drinking water purchased from a store in Mahamakut Building, Chulalongkorn University were used as real samples for analysis. The drinking water samples were spiked with hydrogen peroxide to obtain 5 mM and 10 mM H<sub>2</sub>O<sub>2</sub> solutions. A calibration curve was plotted using the IPDPR/DPR ratio of the 20:10 ppm AgNSs/NPrs sensor after treatment with standard H<sub>2</sub>O<sub>2</sub> solution with concentrations ranging from 0.625 mM to 15 mM. Concentrations of the spiked samples were calculated using the linear regression equation of the calibration plot. %Recovery and %RSD were calculated to evaluate the accuracy and precision of the dual-shaped plasmonic sensor for real sample analysis. The experiment was conducted for two consecutive days (n=5) for the second drinking water sample to obtain inter-day %Recovery and %RSD values.

## Chapter IV Results and Discussion

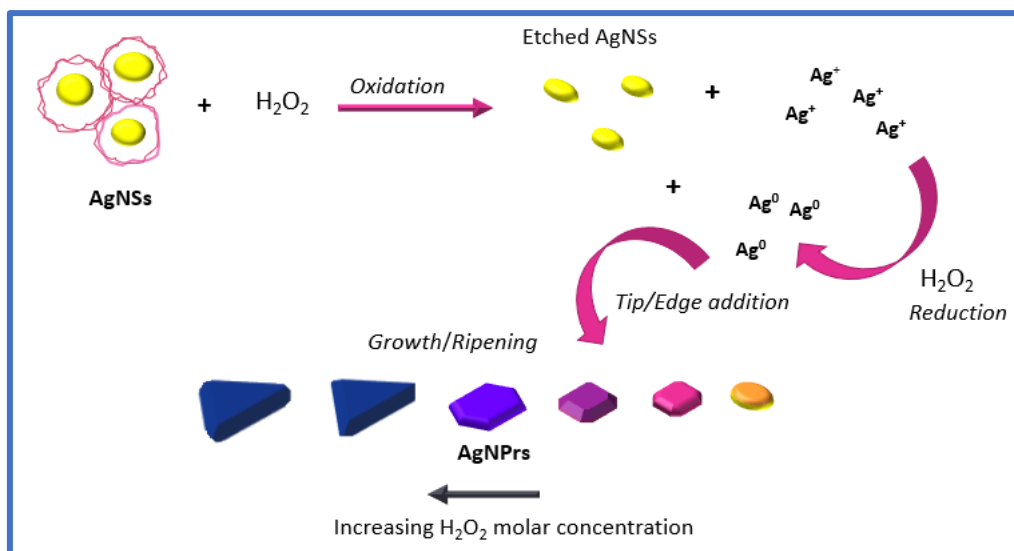
### 4.1 Preparation of Silver Nanospheres (AgNSs)

Silver nanospheres were synthesized by a chemical reduction method. Silver ions from silver nitrate is reduced by sodium borohydride ( $\text{NaBH}_4$ ) into silver metal nuclei that coalesces and forms silver nanospheres. Starch, as a stabilizer, sequesters  $\text{Ag}^+$  by an ion-dipole interaction of the ether and hydroxyl oxygens, preventing  $\text{Ag}_2\text{O}$  formation.<sup>29</sup> The silver nanospheres colloid appeared dark brown in color immediately after mixing of  $\text{AgNO}_3$  and  $\text{NaBH}_4$  due to the enhanced absorption as the nanospheres were formed.

### 4.2 Preparation of Silver Nanoprisms (AgNPrs)

Hydrogen peroxide plays a key role in the transformation of nanospheres to nanodisks and nanoprisms.<sup>31</sup> It promotes the formation of planar twinned seeds from silver nanospheres, removes unstable particles by oxidative etching and then reduce silver ions that nucleates on the seeds. By varying the hydrogen peroxide concentration, silver nanoprisms of different size, shape, and colors can be obtained as shown in **Figure 4.1**.<sup>29</sup>

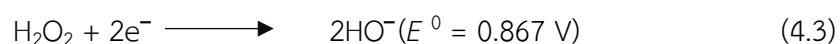
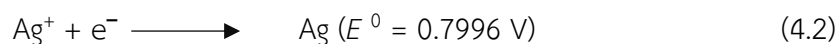


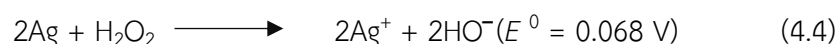


**Figure 4.1** Schematic diagram of the synthesis of silver nanoprisms.

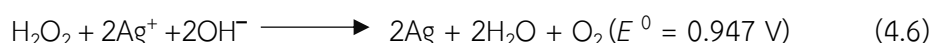
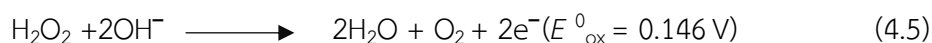
Red silver nanoprisms (1:10 molar ratio of Ag to H<sub>2</sub>O<sub>2</sub>) were chosen as the seeds to achieve the wide color transition range from yellow, orange, red, purple, and blue. In this research, the AgNSs and AgNPrs syntheses follow the method described by Paraklang et al. (2013)<sup>29</sup>. Oxidative etching by hydrogen peroxide transformed the silver nanospheres to nanoprisms. According to the following equations, it is theoretically possible that H<sub>2</sub>O<sub>2</sub> can act as an oxidative etchant of silver nanospheres and a reducing agent for silver ions at the same time as shown in the positive values of **Equations 4.4** and **4.6**. Reduction is more favorable in basic conditions.

H<sub>2</sub>O<sub>2</sub> as an oxidizing agent:





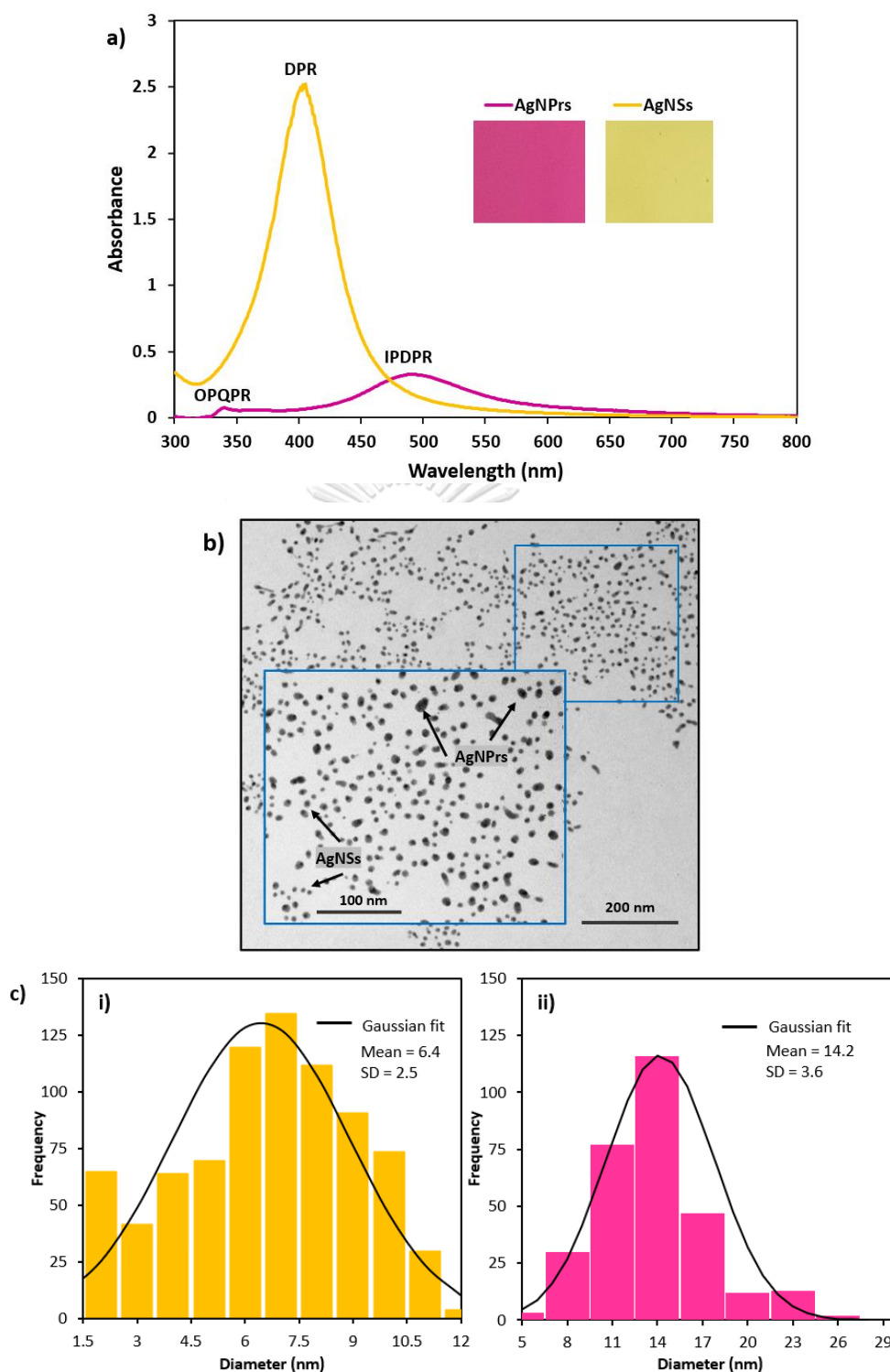
$\text{H}_2\text{O}_2$  as a reducing agent:



Citrate from trisodium citrate was mixed with the AgNPrs in a centrifuge tube. The mixture was allowed to self-assemble for three hours in room temperature. This study exploits the preferential binding of citrate on the Ag(111) facet to control the anisotropic lateral growth of AgNPrs. Citrate protects the Ag(111) facet of the nanocrystal from oxidative etching and isotropic growth, and promotes crystal growth along the Ag(100) surface, hence controlling the shape of the AgNPs.<sup>64</sup> Maintaining the thickness of the nanoprisms while the lateral side is growing is the key to the LSPR redshift which generates the variety of colors.<sup>80, 81</sup> Jiang et al. (2010)<sup>59</sup> reported that citrate has reducing, stabilizing, and complexing ability; although the reducing power is weaker than ascorbic acid or sodium borohydride and the stabilizing property weaker than the surfactants used in their experiments. Additionally, excess citrate can also slow down nucleation through formation of a silver complex. In this work, the silver nanoprisms were centrifuged and washed three times to remove free citrate that can hinder the growth process.<sup>59</sup>

### 4.3 Characterization of Silver Nanoparticles

The successful synthesis of silver nanospheres (AgNSs) was confirmed by UV-Vis spectrophotometry and TEM imaging. The AgNS extinction spectra registered a sharp dipole plasmon resonance band (DPR) at 403 nm (**Figure 4.2a**). The diluted colloid has a bright yellow color (**inset**). The presence of out-of-plane quadrupole resonance (OPQPR) at 339 nm and in-plane dipole plasmon resonance (IPDPR) at 487 nm indicates the successful transformation of silver nanospheres to nanoprisms (**Figure 4.2a**). OPQPR relates to the thickness while the IPDPR related to lateral size or diameter of the of the silver nanoprisms.<sup>82</sup> The colloid was pink in color after dilution (**inset**). Using ImageJ analysis of the TEM micrographs (**Figure 4.2b**), the mean diameters of the nanospheres (807 particles) and nanoprisms (300 particles) were found to be  $6.4 \pm 2.5$  (**Figure 4.2c(i)**) and  $14.2 \pm 3.6$  nm (**Figure 4.2c(ii)**). TEM also confirmed the presence of silver nanoprisms with varying morphologies, specifically elongated plates, and circular disks.



**Figure 4.2** a) Extinction spectra of AgNSs (20 ppm) and AgNPrs (20 ppm) (inset: images of yellow AgNSs and red AgNPrs), b) TEM micrograph of mixed AgNSs/NPrs sensor c) and size distribution histogram of (i) AgNSs and (ii) AgNPrs.

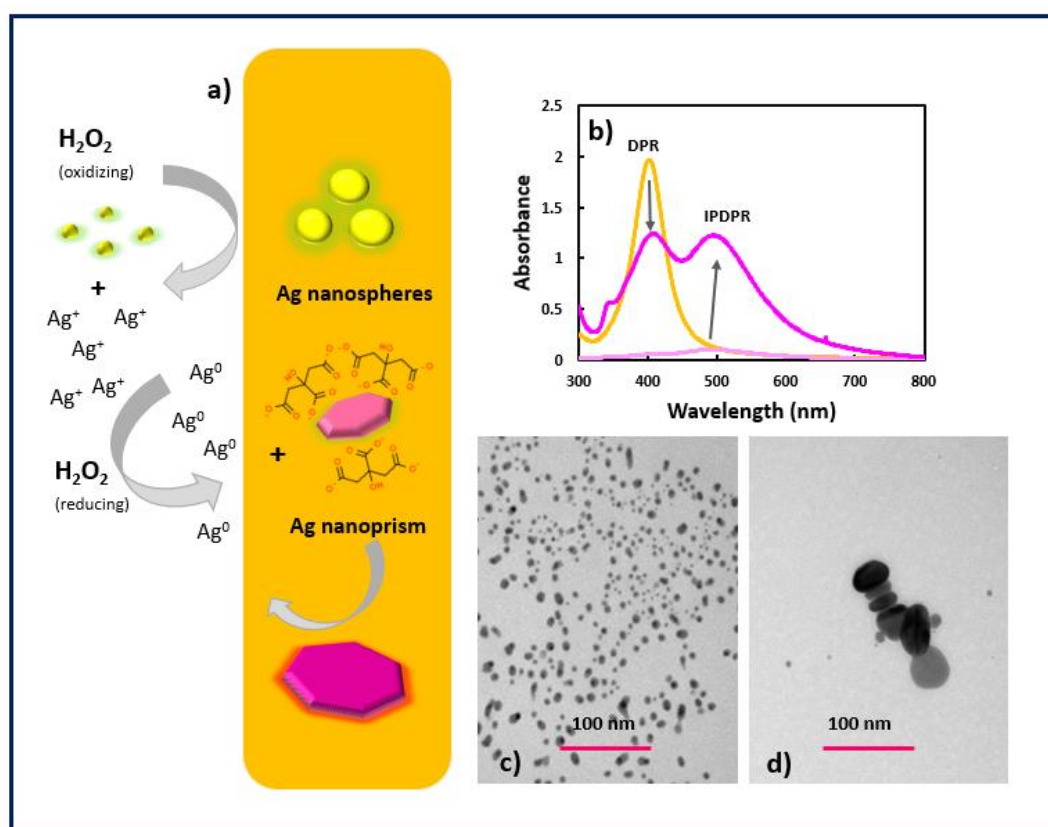
## 4.4 Detection of Hydrogen Peroxide Using a Dual-Shaped Plasmonic Silver Nano-Sensor

### 4.4.1 Preliminary studies using concentrated hydrogen peroxide

In this work, hydrogen peroxide's unique ability to oxidize and reduce silver was exploited to develop a highly selective and sensitive sensor. The sensor consists of starch-stabilized silver nanospheres and citrate-capped silver nanoprisms (AgNSs/NPrs). Silver nanospheres serve as the source of silver ions that are released from oxidation by hydrogen peroxide. Subsequently, hydrogen peroxide reduces these ions to silver metal that can deposit onto the edges of the nanoprism seeds (**Figure 4.3a**). Citrate molecules protect the <111> facet of the AgNPrs from silver deposition and hydrogen peroxide oxidation allowing lateral growth. This results in intensity enhancement and redshift of the plasmon band (**Figure 4.3b**) and a distinct color change. By measuring these spectral and color changes, quantification of hydrogen peroxide is made possible. TEM imaging also confirms the evident growth of the AgNPrs and decrease in the number of AgNSs from **Figure 4.3c** to **Figure 4.3d**.

The redshift of the extinction spectra alone was initially attributed to the growth of the silver nanoprisms. The AgNSs/NPrs sensor, after treatment of H<sub>2</sub>O<sub>2</sub> and dilution, should have an IPDPR  $\lambda_{\max}$  greater than the IPDPR  $\lambda_{\max}$  of the AgNPrs seeds to confirm the growth as shown in **Figure 4.3b**. Thus, the growth of the nanoprism from the dual-shaped sensor was initially only observed at two conditions: (1) high

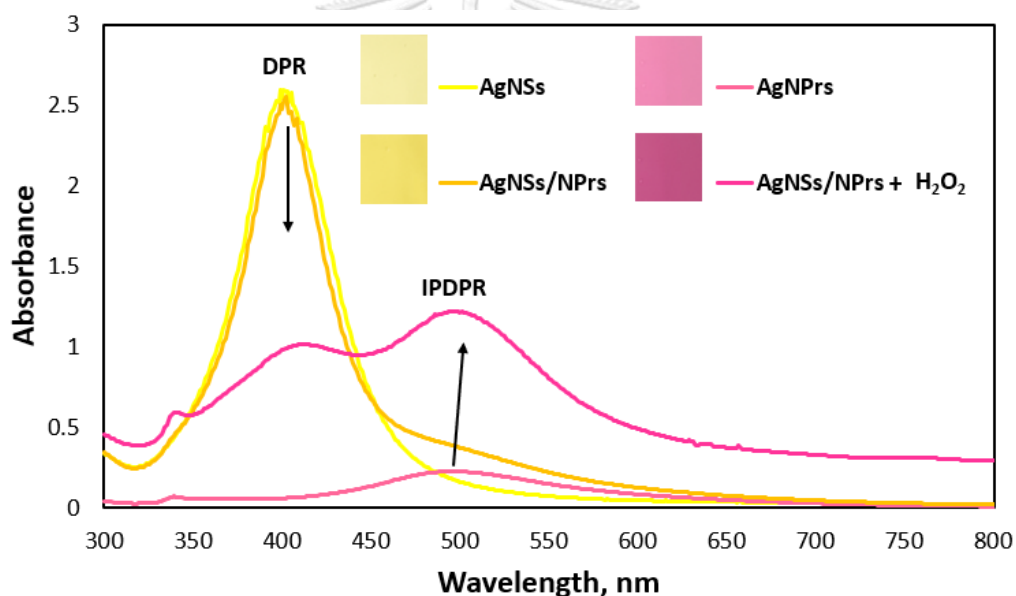
concentrations of silver nanospheres and (2) addition of concentrated hydrogen peroxide. The molar ratio and concentration of the dual-shaped sensor for the initial investigations were 2.5:1 and 97.5:39 ppm (AgNSs:AgNPrs) respectively, which was treated with concentrated hydrogen peroxide.



**Figure 4.3** a) Schematic diagram of the growth-based sensing of hydrogen peroxide using dual-shaped silver nanoparticles. b) Extinction spectra and TEM micrographs of the sensor c) before and d) after addition of concentrated hydrogen peroxide.

As revealed by the extinction spectra in **Figure 4.4**, the dipole plasmon resonance (DPR) at around 400 nm decreased while the intensity of the in-plane dipole plasmon resonance (IPDPR) of the sensor increased more than five times upon

addition of concentrated  $H_2O_2$ . This results in a change in color from yellow to deep red (inset). The table in **Figure 4.4** compares the IPDPR peak wavelength and intensity of the AgNPrs and the sensor after addition of hydrogen peroxide. In hindsight, the color intensity would not only depend on the redshift but would be manifested through the enhancement of extinction intensity. Tracking of the intensities of diminishing DPR and rising IPDPR would be easier and make ratiometric analysis possible which could allow a more sensitive measurement.



**Figure 4.4** The extinction spectra of AgNSs, AgNPrs, AgNSs/NPrs sensor before and after addition of hydrogen peroxide and their individual colors when diluted and (inset) comparison of IPDPR  $\lambda_{max}$  and IPDPR absorbance intensity of the silver nanoprisms and the sensor after addition of 2.5  $\mu L$  of concentrated hydrogen peroxide.

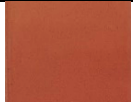








#### 4.4.2 Effect of Silver Nanoprism Seeds

It is possible that the growth could occur using only silver nanospheres (AgNSs) since AgNSs are transformed to AgNPrs with concentrated hydrogen peroxide and high AgNSs concentrations. It is hypothesized that in the presence of AgNPrs seeds can promote its growth even at lower concentrations of AgNSs. To prove this assumption and to ensure that the growth happens on the citrate-capped AgNPr seeds and not on the silver nanospheres, the reactions of AgNSs/NPrs sensor and lone AgNSs were compared by adding 1, 4, and 10  $\mu\text{L}$  of concentrated hydrogen peroxide. **Table 4.1** reveals that no color change is observed when only silver nanospheres of the same concentration (98 ppm) as used in the AgNSs/NPrs sensor are present after reaction with concentrated hydrogen peroxide. The AgNSs/NPrs sensor, on the other hand, generated red orange, reddish purple, and purple colors. When the concentration of the AgNSs was doubled (196 ppm), the growth was observed at 4  $\mu\text{L}$  of  $\text{H}_2\text{O}_2$  as revealed by the orange color. At higher concentrations of AgNSs, growth can occur with  $\text{H}_2\text{O}_2$  because the collision probability of the nanoparticles increases leading to Ostwald ripening.<sup>29</sup> The growth on hydrogen peroxide sensors with lower concentration of AgNSs was not observed previously.<sup>69, 71</sup> This is a simple proof that the citrate-capped AgNPr seeds enabled the sensitive, growth-based detection of hydrogen peroxide by facilitating particle enlargement. Etching by hydrogen peroxide on seed-mediated synthesis removes the relatively



unstable silver nanospheres, leaving the highly stable citrate ligand-capped to promote the nucleation process on its lateral side.<sup>32</sup>

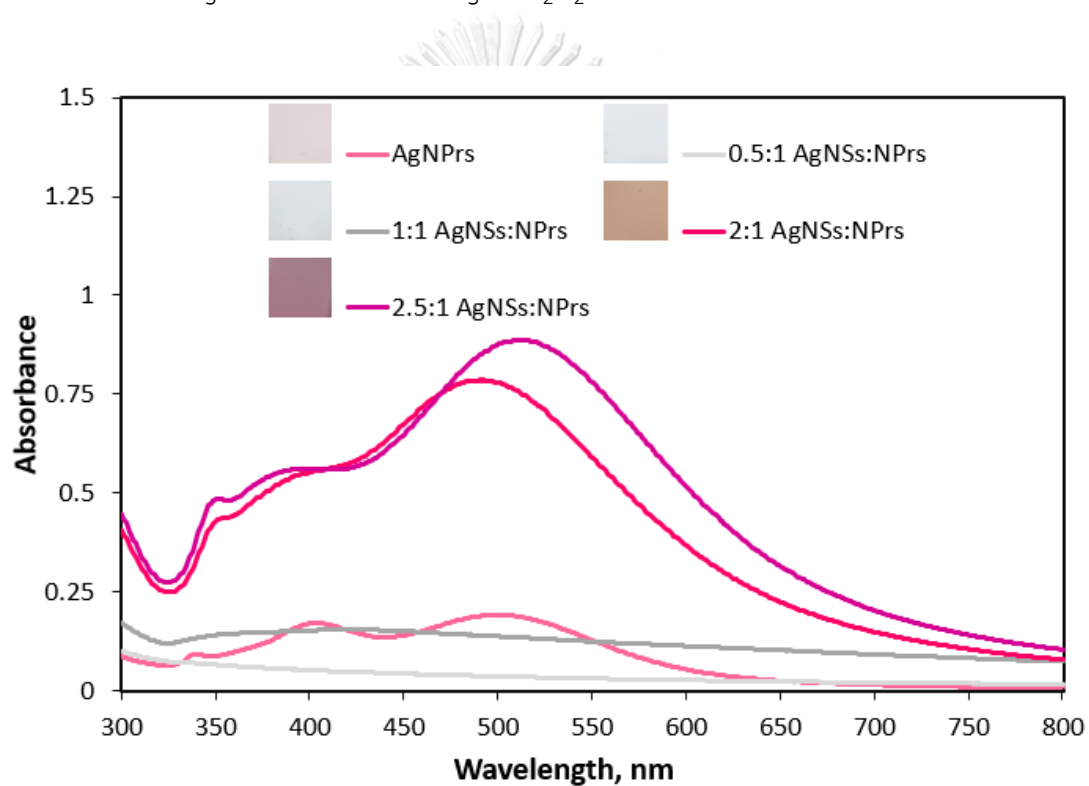
**Table 4.1.** Digital images of the diluted dual-shaped silver nanoparticle sensor and lone silver nanospheres after reacting with concentrated  $H_2O_2$ .

Silver nanoparticles	Concentrated $H_2O_2$ volume		
	1 $\mu$ L	4 $\mu$ L	10 $\mu$ L
AgNSs/NPrs (98/39 ppm)			
AgNSs (98 ppm)			
AgNSs (196 ppm)			

#### 4.4.3 Effects of AgNSs to AgNPrs ratio and concentration

The AgNSs/NPrs sensors with ratios of 0.5:1 to 2.5:1 (AgNSs:AgNPrs) were mixed with 2.5  $\mu$ L of concentrated hydrogen peroxide. **Figure 4.5** shows that the highest IPDPR and OPQPR intensities and a redshift were observed at 2.5:1 which signifies that growth of the AgNPrs occurs at higher concentrations of AgNSs. At a 2:1 (AgNSs:AgNPrs) ratio, in-plane dipole plasmon resonance and of out-of-plane quadrupole plasmon resonance also significantly increased which also suggest growth of the silver nanoprisms. On the other hand, lower concentrations of AgNSs (0.5:1 and 1:1) would yield a flat spectra thus the opalescent white color indicating the consumption of silver nanospheres. Therefore, an excess AgNSs concentration would

be needed to trigger nanoparticle growth since it is the source of silver ions. This would also mean that the 2:1 (78:39 ppm) AgNSs:NPrs ratio is sufficient to carry out the enlargement of AgNPrs which would reduce chemical consumption. Furthermore, very high AgNSs signal could mask the IPDPR growth signal when smaller concentrations of hydrogen peroxide are present. Therefore, the 2:1 ratio would ensure sensitive growth-based sensing of  $H_2O_2$ .



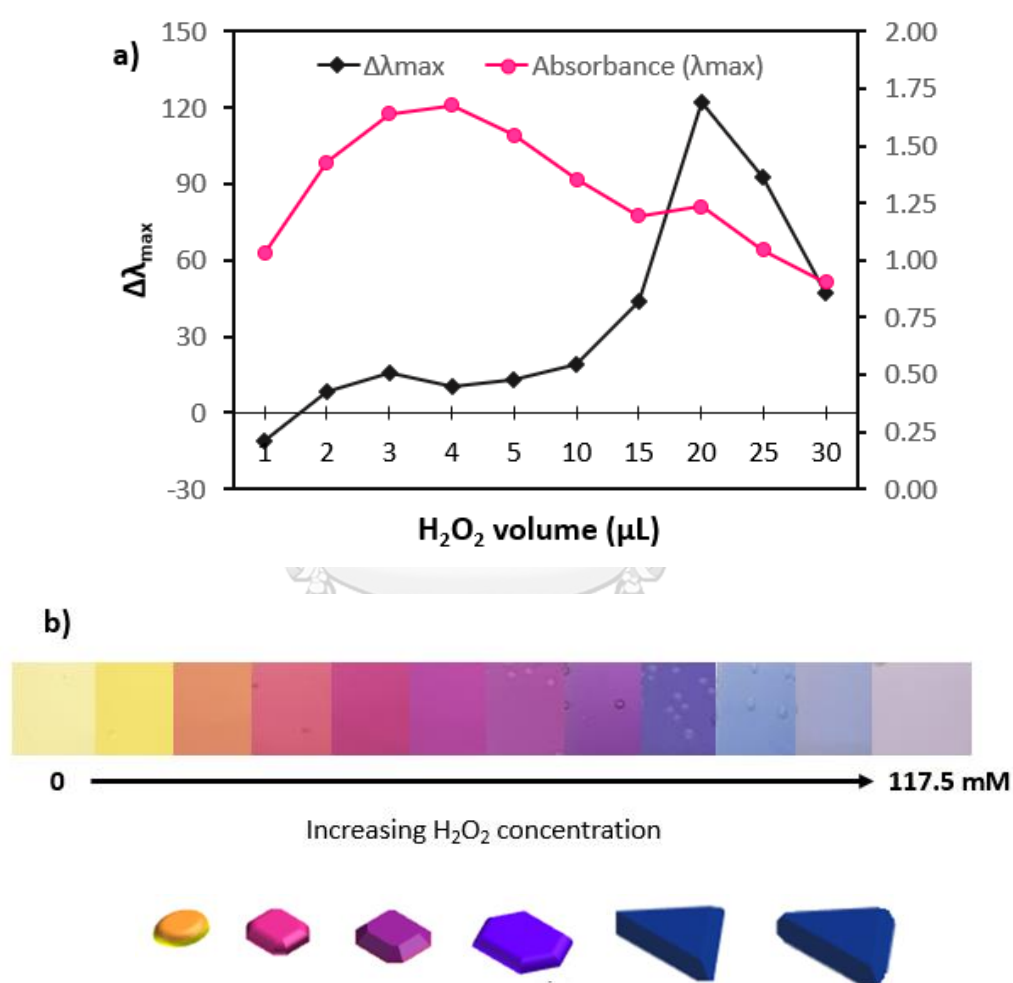
**Figure 4.5** Extinction spectra of the AgNPrs and AgNSs/NPrs sensor with varying silver nanospheres concentration after addition of concentrated hydrogen peroxide. Inset: images of diluted AgNPrs and treated AgNSs/NPrs sensors.

#### 4.4.4 Effect of Volume of Concentrated Hydrogen Peroxide

The effect of volume of  $\text{H}_2\text{O}_2$  concentration on the AgNSs/NPrs (78:39 ppm) sensors was investigated by reacting the sensors with various volumes of concentrated  $\text{H}_2\text{O}_2$ . As shown in **Figure 4.6a**, as hydrogen peroxide volume increases, absorbance intensities at the IPDPR  $\lambda_{\text{max}}$  also increases until it achieved the maximum value at 4  $\mu\text{L}$  (final  $\text{H}_2\text{O}_2$  concentration with sensor: 15.7 mM). This indicates the transformation of silver nanospheres to silver nanoplates or nanoprisms while the AgNPrs that was initially present was also increasing in lateral length. The maximum absorbance point can be related to the total conversion of AgNSs to AgNPrs.<sup>82</sup> The absorbance intensities start to diminish at  $\text{H}_2\text{O}_2$  concentrations beyond 4  $\mu\text{L}$  because hydrogen peroxide starts to consume the smaller plates to promote further growth of the larger AgNPrs. The red-shift indicates the increase in the lateral size of the nanoprisms until it reaches the maximum point at around 20  $\mu\text{L}$  (final  $\text{H}_2\text{O}_2$  concentration with sensor: 78.3 mM) of concentrated hydrogen peroxide when the higher  $\text{H}_2\text{O}_2$  starts to oxidize the silver nanoprisms causing a change in color from light blue to blue gray (**Figure 4.6b**). The maximum absorbance intensity and red-shift corresponds to a red violet and light blue colors (**Figure 4.6b**).

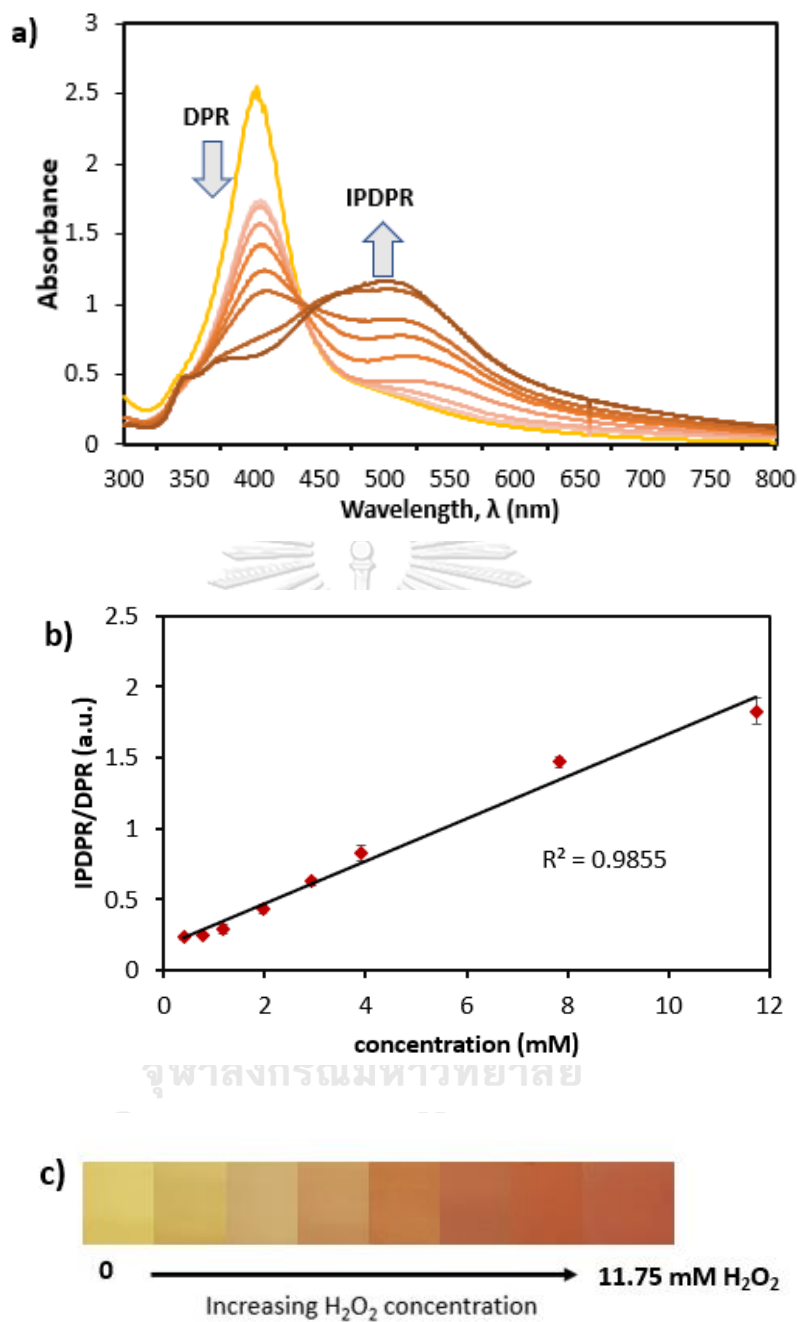
Looking at the plot, a wider linear range can be established at lower concentrations if absorbance at IPDPR  $\lambda_{\text{max}}$  is monitored instead of the redshift or change in IPDPR  $\lambda_{\text{max}}$ . Growth-based sensing with dual-shaped silver nanoparticles also reveals hues from light yellow, golden yellow, orange, red, red violet, purple, to

blue which was not seen previously with AgNPs decomposition-based or even growth-based AuNPs detection.<sup>26, 67, 70, 83, 84</sup> Only etching-based sensing with gold nanorods produced the most number of colors as of this writing.<sup>24, 27</sup> This broad range of colors opens a simple avenue for instrument-free, or semi-quantitative colorimetric analysis of hydrogen peroxide, especially naked-eye detection.



**Figure 4.6** Effect of the volume of concentrated hydrogen peroxide to the a) IPDPR  $\lambda_{max}$  and absorbance intensities with respect to the AgNPs  $\lambda_{max}$  and b) colors generated by the treated sensor after dilution. Inset: shape transformation of AgNPs.

The effect of lower volume of the concentrated hydrogen peroxide to the spectra and color of the sensor was further studied. **Figure 4.7a**, shows the plot of absorbance against the varying volume of concentrated hydrogen peroxide (final concentration: 0.39 mM to 19.6 mM). As the hydrogen peroxide concentration increases, dipole plasmon resonance band decreases while in-plane dipole plasmon resonance increases which can be explained by the etching of silver nanospheres and growth of silver nanoprisms. Linear range was found to be 0.39 to 3.9 mM if only the decrease of the dipole plasmon resonance at 402 nm was recorded. However, using ratiometric analysis (IPDPR/DPR) the linear range extends up to 11.75 mM (**Figure 4.7b**). The computed detection limit is 4.8  $\mu\text{M}$  based on the  $3\sigma/\text{slope}$ , where  $\sigma$  is the standard deviation of blanks. At this lower concentration range, a distinct transition of colors was still observed from yellow, orange, to red orange (**Figure 4.7c**).



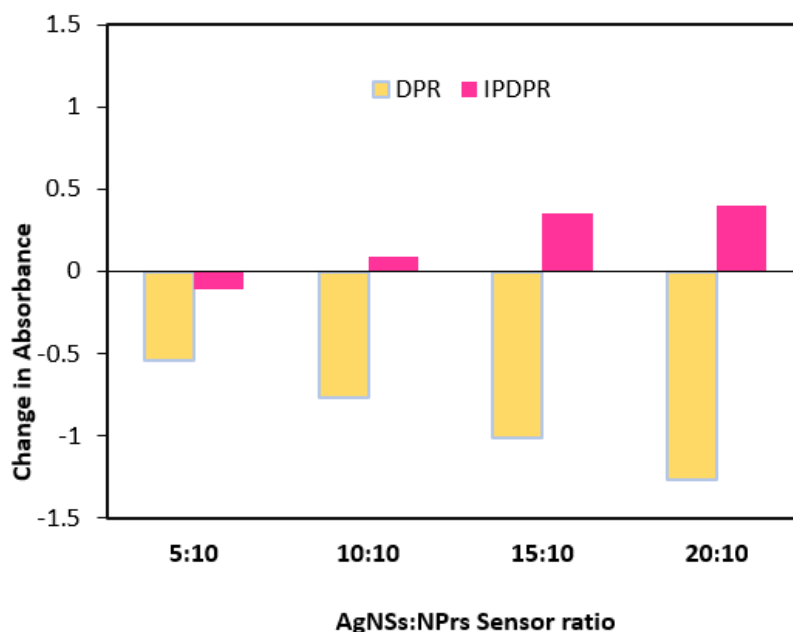
**Figure 4.7** a) Extinction spectra of the sensor treated with different volumes of concentrated hydrogen peroxide. b) A calibration plot of  $H_2O_2$  concentration against the ratio of IPDPR and DPR. c) Digital images of color transition generated in this linear range.

#### 4.5 Optimization of the Sensor for the Diluted H<sub>2</sub>O<sub>2</sub> Detection

The previous experiments were able to achieve a sub-micromolar detection limit; however, it was hypothesized that it can still be improved and simplified. The dilution step can be removed by utilizing lower concentrations of the AgNSs/NPrs sensor. This can be used for low levels or diluted hydrogen peroxide which can consequently improve the limit of detection.

##### 4.5.1 Effect of AgNSs/NPrs ratio

The maximum concentration of AgNSs that can be employed without errors due to very high absorbance is 20 ppm. Starting with 10 ppm baseline concentration of citrate-capped AgNPrs, the responses of AgNSs to AgNPrs sensor ratios (0.5:1 to 2:1) with 50  $\mu$ L of 9.79 mM hydrogen peroxide was investigated. As expected, the highest increase in IPDPR was found at 20:10 ppm sensor ratio (**Figure 4.8**) due to higher available silver that can be etched and regenerated for the growth of the AgNPrs.


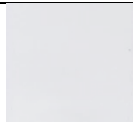








**Figure 4.8** A plot of the change in DPR and IPDPR absorbance after addition of 50  $\mu$ L 9.79 mM hydrogen peroxide into different AgNSs:NPrs sensor ratio.

**Table 4.2** displays the color change of the sensor after treatment of the 9.79 mM  $H_2O_2$ . The AgNSs/NPrs ratio of 0.5:1 completely faded, while the 2:1 sensor gave the brightest color. The color is more vibrant in a 2:1 sensor ratio compared to other ratios because there are more silver nanospheres remaining after the reaction and bigger nanoprisms are present as indicated by the higher IPDPR peak. Accordingly, the 2:1 sensor ratio was used for the succeeding experiments.



**Table 4.2** Digital images of sensors with varying AgNSs:NPrs ratios before and after treatment of 9.79 mM hydrogen peroxide (50  $\mu$ L).

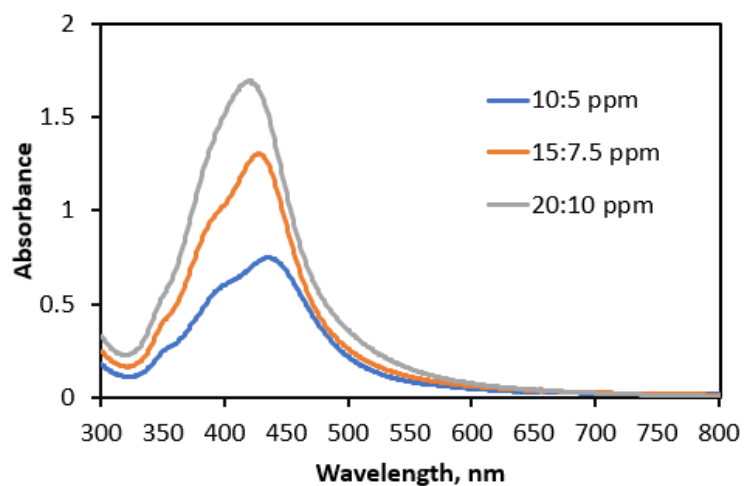
AgNSs/NPrs sensor ratio	Color	
	Original Sensor	Treated Sensor
0.5:1 (5:10 ppm)		
1:1 (10:10 ppm)		
1.5:1 (15:10 ppm)		
2:1 (20:10 ppm)		

#### 4.5.2 AgNSs/NPrs concentration

Using 2:1 AgNSs:AgNPrs ratio, the effect of lower concentration was also studied. **Figure 4.9** shows the spectra of the 10:5, 15:7.5 and 20:10 ppm after the addition of 50  $\mu$ L  $H_2O_2$ . The growth of the nanoprisms, as indicated by the IPDPR, is still higher at 20:10 ppm of the sensor. Again, this is due to greater availability of the silver ions from the 20 ppm AgNSs. In terms of visual observation, this would also relate to the darker color of the sensor as shown in **Table 4.3**.

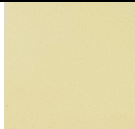
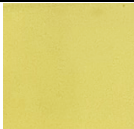




Low AgNSs/NPrs sensor concentration allows the detection of low hydrogen peroxide concentrations and removal of the dilution step which further

simplifies the work. However, at low sensor concentrations, the color transition is not clear thus, it would not be sufficient for colorimetric detection by the naked-eyes.



**Figure 4.9** Extinction spectra of 2:1 AgNSs/NPrs sensor ratio with different concentrations (ppm) after treatment of 9.79 mM of hydrogen peroxide.

**Table 4.3** Digital images of sensors with different concentrations at 2:1 AgNSs:NPrs ratio before and after treatment of 9.79 mM hydrogen peroxide (50  $\mu$ L).

AgNSs/NPrs sensor concentration (ppm)	Color	
	Original Sensor	Treated Sensor
10:5		
15:7.5		
20:10		

## 4.6 Analytical Performance

### 4.6.1 Analytical figures of merit

The effect of the higher nanoparticle concentration with the 2:1 (AgNSs:NPrs) ratio on the colors and performance of the AgNSs/NPrs sensor was investigated. Calibration curves were obtained by plotting concentrations of diluted hydrogen peroxide (0.625 mM to 4000 mM) versus the ratio of IPDPR to DPR obtained from UV-Vis measurement of the treated sensor. **Figure 4.10** illustrates the linear ranges of the 20:10 ppm and 80:40 ppm AgNSs/NPrs sensors. **Table 4.4** summarizes the sensitivity (slope), linear range, detection limit (LOD) and limit of quantitation (LOQ) of the AgNSs/NPrs sensor with increasing concentrations. The 20:10 ppm ratio achieved the highest sensitivity and lowest limit of detection. However, this yielded the shortest linear range. The dynamic linear range of the AgNSs/NPrs sensor was found to broaden as the sensor concentration is increased. A higher number of AgNSs and AgNPrs particles would translate to a steady supply of silver ions and seeds that could grow as the hydrogen peroxide increases. Lower concentration results in a shorter linear range because upon increase of hydrogen peroxide the silver nanospheres get consumed through oxidation and eventually would also dissolve the AgNPrs. In addition, the linear range of the 80:40 ppm AgNSs/NPrs concentration is limited by the evolution of bubbles that can affect light scattering causing the deviation from linearity at high hydrogen peroxide concentrations (**Figure 4.10b**). A four-fold increase in sensor concentration results in more than 50 times expansion of

the linear range. Reducing the concentration of the sensor would lead to a more sensitive measurement and lower detection limit. In terms of colorimetric measurement, the 80:40 ppm ratio generated very distinct colors from yellow, orange, red to purple that would allow semi-quantitative determination of  $\text{H}_2\text{O}_2$  across a wide dynamic linear range (**Figure 4.11**). Although it would still require dilution for UV-Vis measurements, optical readout can be performed with ease, especially with paper-based analytical devices. Based on the results, the developed dual-shaped plasmonic sensor offers a flexible linear range that can measure a wide variety of hydrogen peroxide concentrations present in many industries using UV-Vis spectrophotometry and colorimetric readout by the naked eyes.



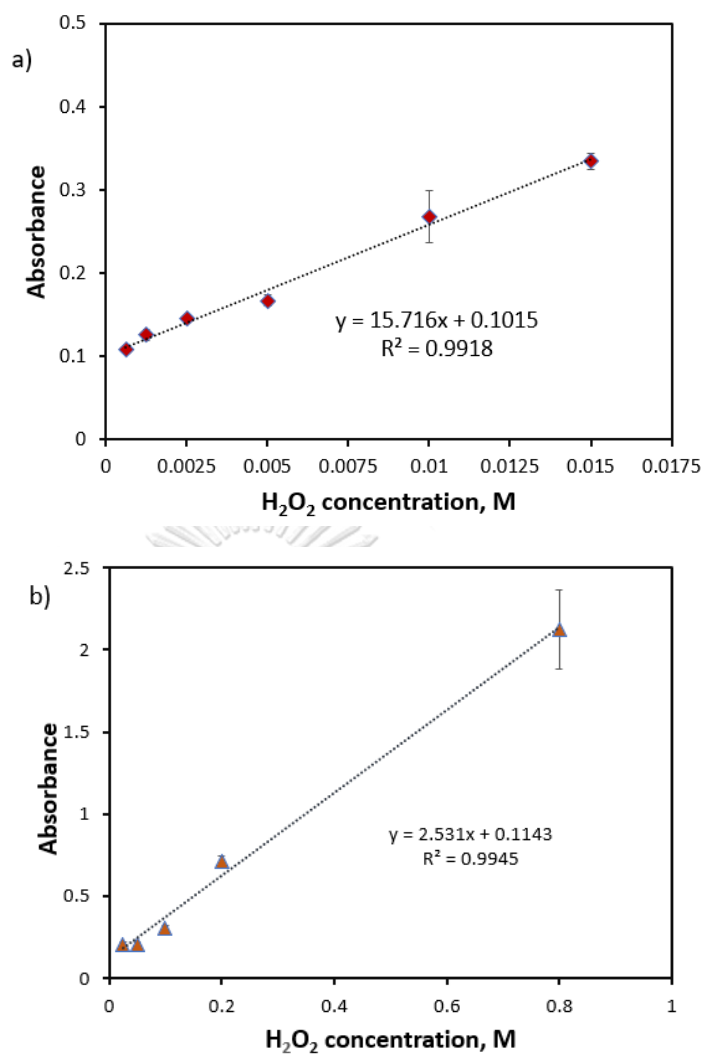
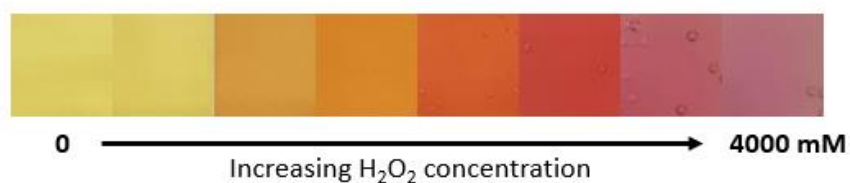


Figure 4.10 Plots of the linear ranges of the a) 20:10 ppm and b) 80:40 ppm AgNSs/NPrs sensors.

Table 4.4 The analytical figures of merit obtained from different 2:1 AgNSs:NPrs concentrations.

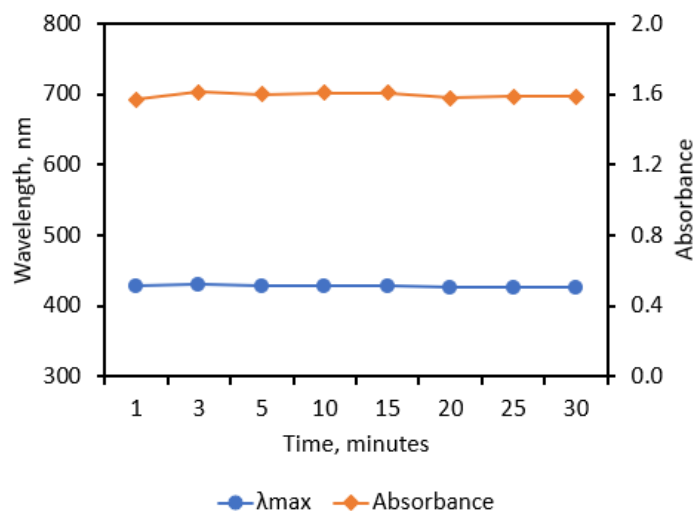
AgNSs:NPrs ratio (concentration, ppm)	$R^2$	slope	Linear range (mM)	LOD (mM)	LOQ (mM)
20:10	0.9918	15.716	0.2 to 15	0.2	0.5
40:20	0.9943	5.2889	0.3 to 150	0.3	0.8
60:30	0.9931	3.4159	0.2 to 400	0.2	0.7
80:40	0.9945	2.531	10 to 800	10	30



**Figure 4.11** Digital images of the 80:40 ppm AgNSs/NPrs sensor after treatment with increasing hydrogen peroxide concentration.

#### 4.6.2 Response time

Optimum response time was investigated by monitoring the IPDPR  $\lambda_{\max}$  and intensity of the 20:10 ppm silver nanoparticle sensor after addition of hydrogen peroxide (9.79 mM, 50  $\mu$ L). **Figure 4.12** demonstrates that the  $\lambda_{\max}$  and absorbance intensities remained constant after one minute. This is due to the rapid Ag-H<sub>2</sub>O<sub>2</sub> redox reaction that immediately takes place upon contact. This makes the AgNSs/NPrs sensor more beneficial for routine work compared to other colorimetric analysis that requires longer incubation time.



**Figure 4.12** Effect of the response time on the IPDPR  $\lambda_{\max}$  and absorbance intensity after addition of  $\text{H}_2\text{O}_2$ .

### 4.6.3 Selectivity Test

#### 4.6.3.1 Effect of common anions

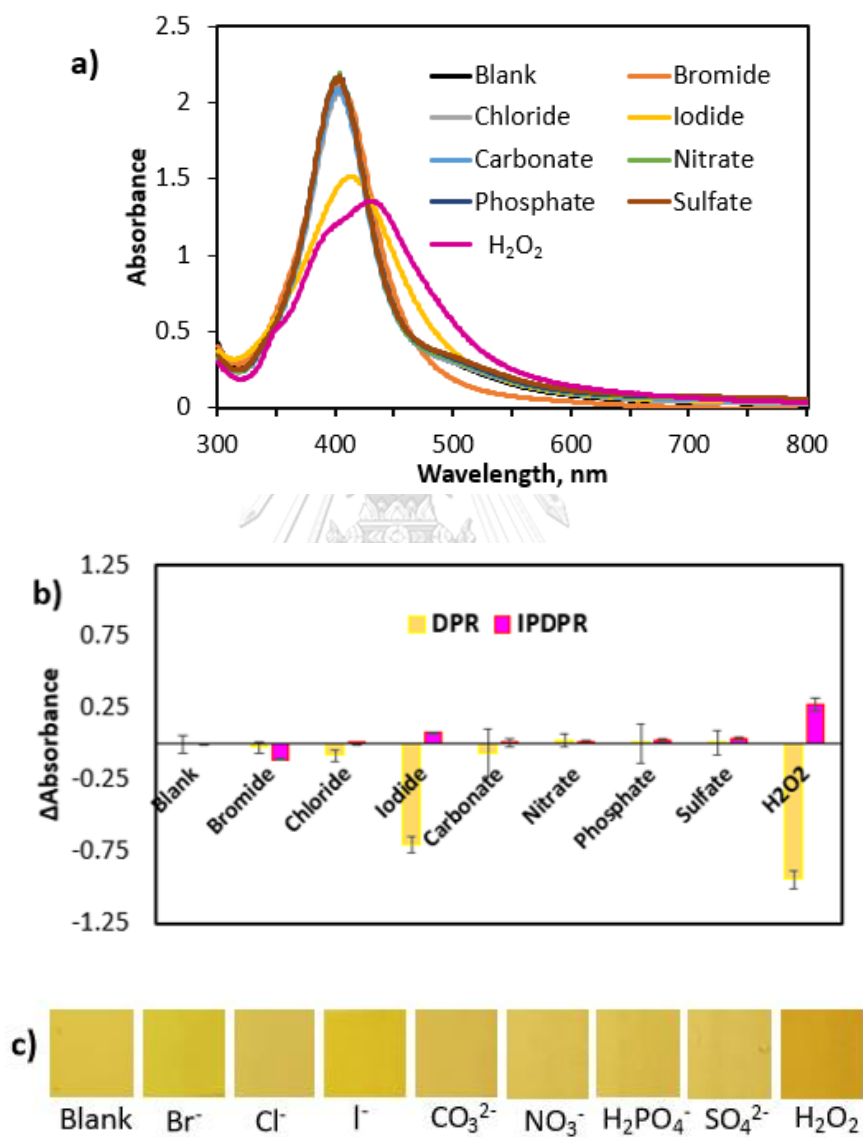
Common anions specifically bromide, chloride, iodide, carbonate, nitrate, dihydrogen phosphate and sulfate were tested against the specificity of the 20:10 ppm AgNSs/NPrs sensor. Halides are known to etch and form insoluble compounds with silver.<sup>17, 85</sup> Other anions may displace the citrate molecules on the surface of the AgNPrs and thus make it vulnerable to etching by hydrogen peroxide and halides. These anions can also coordinate with silver ions released upon oxidation of silver nanospheres and prevent the growth of the nanoprisms.<sup>86-89</sup>

**Figure 4.13a** shows the extinction spectra of the AgNSs/NPrs sensor before (blank) and after addition of 50  $\mu\text{L}$  of 1 mM of the anions. Iodide was also

able to reduce the dipole plasmon resonance band of the sensor significantly aside from hydrogen peroxide. Additionally, the shoulder of the spectrum of the sensor with bromide is lower compared to the rest. **Figure 4.13b** reveals the extent of change of the DPR and IPDPR measured at 403 and 498 nm, respectively after addition of the anions (1 mM) and H<sub>2</sub>O<sub>2</sub> (20 mM) using the blank sensor's DPR and IPDPR as the reference point. A positive change of the IPDPR (498 nm) indicates a growth of nanoprisms, on the other hand, a DPR decrease (403 nm) implies etching of the silver nanospheres. Only bromide and iodide seem to significantly affect the sensor's color (**Figure 4.13c**) as observed by naked eyes. Results suggest that at 1 mM concentration, iodide was able to induce etching and growth of the AgNPs while bromide have potentially degraded the silver nanoprisms. According to Espinoza et al. (2012)<sup>85</sup>, halides participate in two competing reactions, namely oxidative etching and aggregation of silver nanoparticles. Chloride decomposes AgNPs very slowly at concentration less than 27 mM which is why a small decrease in DPR is observed. Bromide and iodide concentrations in fresh waters or biological matrices are in sub-micromolar range<sup>90-93</sup>; therefore, they are not considered as a major concern if their concentrations in real samples are less than 1 μM. Hydrogen peroxide's concentration in blood plasma is around 1 to 5 μM<sup>94</sup> while household and industrial use varies from 0.05% to 40% (w/v)<sup>95-98</sup>. On the contrary, chloride is present in higher concentrations in nature. For example, the concentrations of chloride in humans sweat and blood serum are around 20 to 40 mM, and 97 to 107 mM respectively.<sup>99</sup>



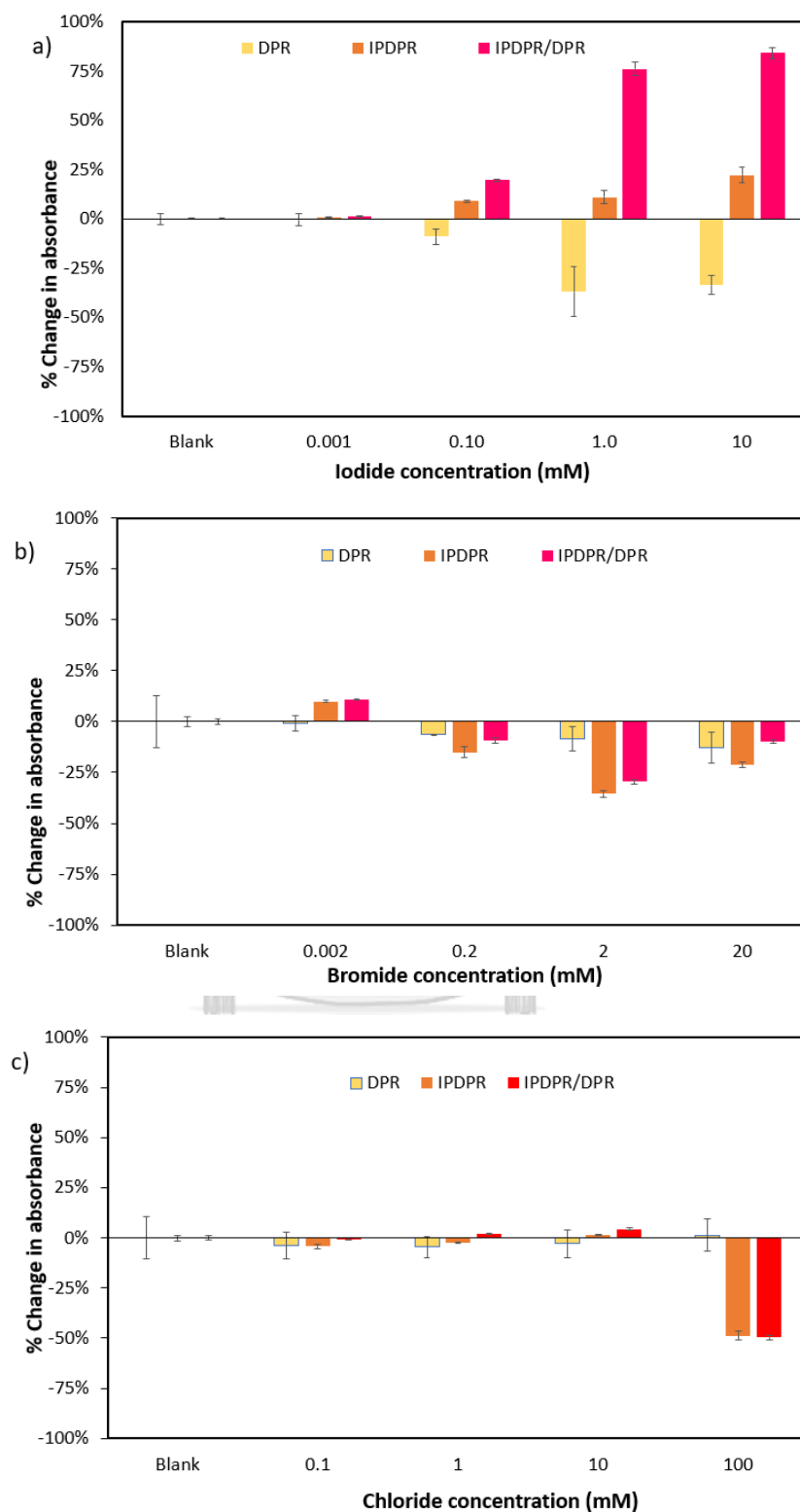
Seawater chloride concentration is around  $5.59 \times 10^2 \text{ M}^{100}$ . Thus, tolerance tests for these halides are still necessary to confirm the robustness of the sensor against these anions.



**Figure 4.13** a) Extinction spectra, b) change in absorbance, and c) digital images of the 20:10 sensor before (blank) and after addition of the anions and  $\text{H}_2\text{O}_2$ .

#### 4.6.3.2 Tolerance test for halides

Halide solutions with concentration from  $10^{-6}$  M to  $10^2$  M were prepared and mixed (50  $\mu$ L) with the 20:10 ppm AgNSs/NPrs sensor. The absorbance values of DPR, IPDPR and the IPDPR/DPR ratio were recorded after the addition of halides. **Figures 4.14a & 4.14b** reveal that the sensor has a low tolerance limit against iodide and bromide ions (1  $\mu$ M). At 2  $\mu$ M, bromide has a change in its IPDPR/DPR ratio of around 11% which indicates the growth mechanism is observed at this level of bromide. On the other hand, the sensor can tolerate as high as 10 mM of chloride according to **Figure 4.13c**. Etching of the nanospheres occur at low chloride concentrations but the IPDPR and IPDPR/DPR ratio remain stable up to 10 mM. Bottled drinking water was used as a real sample for this study. Bromide and Iodide levels of drinking water are typically present in trace concentrations<sup>101</sup> and should not affect the sensor.



**Figure 4.14** Plots of the DPR, IPDPR and IPDPR/DPR shift after addition of a) iodide, b) bromide, and c) chloride for tolerance study.

#### 4.6.4 Accuracy and Precision

In this study, accuracy and precision were estimated using the reaction of the 80:40 ppm AgNSs/NPrs sensor and concentrated hydrogen peroxide. Ultrapure water was used to adjust the final concentration to 5 and 10 mM of H<sub>2</sub>O<sub>2</sub>. **Table 4.5** demonstrates the high accuracy of the AgNSs/NPrs sensor through the obtained recovery from 94.5% to 102.3%. Intra-day and Inter-day measurements were done to investigate precision. Precision was found to be also high at less than 2.5% relative standard deviation (RSD). Results imply that sufficient accuracy and precision based on the AOAC guidelines was achieved using the plasmonic dual-shaped silver nanoparticle sensor.

**Table 4.5** Accuracy and precision of the AgNSs/NPrs sensor expressed as %recovery and %relative standard deviation (RSD).

Sample	Added H <sub>2</sub> O <sub>2</sub> (mM)	Intra-day			Inter-day		
		Found (±SD, mM)	%Recovery	%RSD, n=5	Found (±SD, mM)	%Recovery	%RSD, n=2
1	5.0	5.1 (±0.1)	102.3%	1.6	4.7 (±0.1)	94.5%	1.8
2	11.0	11.0 (±0.4)	100.0%	0.6	11.1 (±0.2)	100.9%	2.2

#### 4.6.5 Application to real samples

Real water sample from two different brands of bottled drinking water were spiked with hydrogen peroxide to make 5 and 10 mM of H<sub>2</sub>O<sub>2</sub> solutions. A calibration curve (**Figure 4.10a**) was then created by plotting the IPDPR/DPR ratio values against the concentration of hydrogen peroxide standard solutions (0.625 to

15 mM). The sample solutions were reacted with 20:10 ppm AgNSs/NPrs sensor and their concentration calculated using the linear regression equation from the calibration plot. Results from **Table 4.6** suggest that enzyme-free detection with the developed plasmonic AgNSs/NPrs sensor can determine H<sub>2</sub>O<sub>2</sub> in real drinking water samples with high accuracy and precision. It is suggested that the AgNSs/NPrs sensor should be tested to a variety of real samples.

**Table 4.6** Accuracy and precision of the sensor for analysis of hydrogen peroxide in drinking water samples.

Sample	Added (mM)	Intra-day			Inter-day		
		Found (±SD, mM)	%Recovery	%RSD, n=5	Found (±SD, mM)	%Recovery	%RSD, n=2
1	5	5.1 (±0.1)	101.3	1.1	-	-	-
	10	10.5 (±0.1)	105.5	0.4	-	-	-
2	5	5.0 (±0.01)	100.9	0.3	5.2 (±0.01)	103.5	0.2
	10	10.5 (±0.01)	105.4	0.1	9.9 (±0.01)	98.5	0.1

## Chapter V Conclusion

Herein, a novel, enzyme-free plasmonic sensor for hydrogen peroxide determination was developed using starch-stabilized silver nanospheres (AgNSs) and citrate-capped silver nanoprisms (AgNPrs). AgNSs was successfully synthesized and transformed into AgNPrs as confirmed by UV-Vis spectrophotometry and TEM imaging. In this work, the dual-shaped silver nano-sensor (AgNSs/NPrs) was reacted with hydrogen peroxide triggering an enlargement of AgNPrs. AgNSs are oxidized by hydrogen peroxide into silver ions that are subsequently reduced to silver metals that deposit onto the lateral side of the citrate-capped AgNPrs. This unique oxidizing and reducing capabilities in the presence of hydrogen peroxide makes the detection highly selective. The growth registers as a redshift and intensity enhancement of the in-plane dipole plasmon resonance (IPDPR) band that can be monitored to quantify the concentration of hydrogen peroxide. In addition, brilliant colors from yellow to red, orange, purple, and blue are generated by the sensor as the amount of  $\text{H}_2\text{O}_2$  was increased allowing easy colorimetric readout by the naked eyes. Furthermore, the reaction was carried out in ambient conditions without adjusting pH or temperature. The reaction time of the AgNSs/NPrs sensor is instantaneous that it completes in less than a minute. The detection limit (LOD) of the AgNSs/NPrs reaction with concentrated hydrogen peroxide is  $4.8 \mu\text{M}$ . Ratiometric analysis using the dipole plasmon resonance (DPR) and IPDPR absorbance values made the

measurement more sensitive by extending the dynamic linear range from 3.9 to 11.75 mM. Halides are the only common anions that were found to interfere with the measurements. Hence, tolerance studies were performed to know how much halides can be present in a sample without interference. Results reveal that the AgNSs/NPrs sensor can only tolerate bromide and halide concentrations at around 1  $\mu\text{M}$  due to the ability of these anions to etch and/or grow the silver nanoparticles. For chlorides, the developed sensor can tolerate up to 10 mM. The real sample used in this study was a bottled drinking water which should only contain trace amounts of bromide and iodide, and less than 1 mM of chloride, and therefore should not interfere with the measurement.

To further simplify the detection and allow sensitive measurement with diluted hydrogen peroxide solution, the AgNSs/NPrs sensor was optimized at lower concentrations. The optimum ratio and concentration were found to be 20:10 ppm (AgNSs:NPrs). However, only light to dark yellow color transition was observed for  $\text{H}_2\text{O}_2$  concentrations of less than 20 mM. Hence, using the 2:1 AgNSs:AgNPrs sensor ratio, the effect of higher silver nanoparticle concentrations to the colors and analytical performance of the sensor was also studied. Results demonstrate that increasing the AgNSs/NPrs sensor concentration 4-fold can expand the linear range by more than 50 times. Vibrant colors can be achieved at 80:40 ppm (AgNSs:NPrs) ratio from yellow to orange, red and purple. This would facilitate facile and quick detection of hydrogen peroxide by colorimetric readout by the naked eyes.

Accuracy and precision were investigated using the %recovery and %RSD computation of intra-day (n=5) and inter-day (n=9) measurements of concentrated hydrogen peroxide. Results demonstrate that the AgNSs/NPrs sensing of H<sub>2</sub>O<sub>2</sub> can be accomplished with high accuracy (%recovery: 94.5-102.3) and precision (%RSD: <2.5). Analysis of drinking water spiked with hydrogen peroxide obtained satisfactory accuracy (%recovery: 98.5-105.5) and precision (%RSD: <1.5) according to AOAC guidelines.

In conclusion, the growth-based sensing approach using dual-shaped silver nanoparticles (AgNSs/NPrs) is a feasible alternative to hydrogen peroxide determination since it enables a simple, rapid, highly selective, and sensitive detection. Furthermore, the distinct multi-color transition produced by the sensor enables a quick, on-site, and instrument-free measurement of a wide-range of H<sub>2</sub>O<sub>2</sub> concentrations in many industries with colorimetric readout using the naked eyes.

#### Future Work

The AgNSs/NPrs sensor can be tested to measure concentrations of hydrogen peroxide in commercial products like wound disinfectants, nasal spray, or hand wash. It can also be tested for the hydrogen peroxide detection from cancer cells or urine which have more complex matrices. H<sub>2</sub>O<sub>2</sub> detection from oxidase enzymes is also a possible application for indirect detection of substrates like cholesterol or glucose which have been done using decomposition-based sensing of



silver nanoparticles. Silver nanoprisms protected by other stabilizing agents can also be investigated. Furthermore, growth-based sensing using silver nanoprism as a platform for colorimetric detection of silver or other metal ions, and reducing agents such as ascorbic acid glutathione, and formaldehyde can also be explored. Finally, visual detection of hydrogen peroxide can also be performed with a smartphone via a colorimetric paper-based analytical device.



## REFERENCES

1. Information, N. C. f. B., PubChem compound summary for CID 784, hydrogen peroxide. National Center for Biotechnology Information: 8600 Rockville Pike, Bethesda, MD, 20894 USA, 2004.
2. Abejón, R.; Garea, A.; Irabien, A., Ultrapurification of hydrogen peroxide solution from ionic metals impurities to semiconductor grade by reverse osmosis. *Separation and Purification Technology* **2010**, *76* (1), 44-51.
3. Grisham, M. B., Methods to detect hydrogen peroxide in living cells: Possibilities and pitfalls. *Comparative Biochemistry and Physiology Part A: Molecular & Integrative Physiology* **2013**, *165* (4), 429-438.
4. Pravda, J., Hydrogen peroxide and disease: towards a unified system of pathogenesis and therapeutics. *Molecular Medicine* **2020**, *26* (1), 41.
5. Veal, E. A.; Day, A. M.; Morgan, B. A., Hydrogen peroxide sensing and signaling. *Molecular Cell* **2007**, *26*, 1-14.
6. Liu, Y.; Nie, J.; Niu, J.; Meng, F.; Lin, W., Ratiometric fluorescent probe with AIE property for monitoring endogenous hydrogen peroxide in macrophages and cancer cells. *Scientific Reports* **2017**, *7* (1), 7293.
7. Ni, Y.; Liu, H.; Dai, D.; Mu, X.; Xu, J.; Shao, S., Chromogenic, fluorescent, and redox sensors for multichannel imaging and detection of hydrogen peroxide in living cell systems. *Analytical Chemistry* **2018**, *90* (17), 10152-10158.
8. de la Rica, R.; Stevens, M. M., Plasmonic ELISA for the detection of analytes at ultralow concentrations with the naked eye. *Nature Protocols* **2013**, *8* (9), 1759-1764.
9. Klassen, N. V.; Marchington, D.; McGowan, H. C. E., H<sub>2</sub>O<sub>2</sub> determination by the I<sup>3-</sup> method and by KMnO<sub>4</sub> titration. *Analytical Chemistry* **1994**, *66* (18), 2921-2925.
10. Rubio, C. P.; Cerón, J. J., Spectrophotometric assays for evaluation of Reactive Oxygen Species (ROS) in serum: general concepts and applications in dogs and humans. *BMC Veterinary Research* **2021**, *17* (1), 226.
11. Liu, J.; Dong, Z.-Z.; Yang, C.; Li, G.; Wu, C.; Lee, F.-W.; Leung, C.-H.; Ma, D.-L., Turn-on luminescent probe for hydrogen peroxide sensing and imaging in living cells

based on an iridium(III) complex–silver nanoparticle platform. *Scientific Reports* **2017**, *7* (1), 8980.

12. Luo, C.; Liu, X.; Liu, F.; He, N.; Yu, R.; Liu, X., AgNPs doping the fold carbon nanoflower composite for highly sensitive electrochemical detection of hydrogen peroxide. *Journal of Electroanalytical Chemistry* **2022**, *904*, 115930.

13. Gaikwad, R.; Thangaraj, P. R.; Sen, A. K., Direct and rapid measurement of hydrogen peroxide in human blood using a microfluidic device. *Scientific Reports* **2021**, *11* (1), 2960.

14. Wu, S.; Tan, S. Y.; Ang, C. Y.; Luo, Z.; Zhao, Y., Oxidation-triggered aggregation of gold nanoparticles for naked-eye detection of hydrogen peroxide. *Chemical Communications* **2016**, *52* (17), 3508-3511.

15. Liang, M.; Yan, X., Nanozymes: From new concepts, mechanisms, and standards to applications. *Accounts of Chemical Research* **2019**, *52* (8), 2190-2200.

16. Peng, W.; Li, W.; Han, H.; Liu, H.; Liu, P.; Gong, X.; Chang, J., Development of chromogenic detection for biomolecular analysis. *VIEW* **2022**, *3* (1), 20200191.

17. Phoonsawat, K.; Ratnarathorn, N.; Henry, C. S.; Dungchai, W., A distance-based paper sensor for the determination of chloride ions using silver nanoparticles. *Analyst* **2018**, *143* (16), 3867-3873.

18. Bothra, S.; Kumar, R.; Pati, R. K.; Kuwar, A.; Choi, H.-J.; Sahoo, S. K., Virgin silver nanoparticles as colorimetric nanoprobe for simultaneous detection of iodide and bromide ion in aqueous medium. *Spectrochimica Acta Part A: Molecular and Biomolecular Spectroscopy* **2015**, *149*, 122-126.

19. Yoon, S.-J.; Nam, Y.-S.; Lee, H.-J.; Lee, Y.; Lee, K.-B., Colorimetric probe for Ni<sup>2+</sup> based on shape transformation of triangular silver nanoprisms upon H<sub>2</sub>O<sub>2</sub> etching. *Sensors and Actuators B: Chemical* **2019**, *300*, 127045.

20. Vyas, G.; Bhatt, S.; Paul, P., Synthesis of calixarene-capped silver nanoparticles for colorimetric and amperometric detection of mercury (Hg<sup>II</sup>, Hg<sup>0</sup>). *ACS Omega* **2019**, *4* (2), 3860-3870.

21. Sapyen, W.; Toonchue, S.; Praphairaksit, N.; Imyim, A., Selective colorimetric detection of Cr(VI) using starch-stabilized silver nanoparticles and application for chromium speciation. *Spectrochimica Acta Part A: Molecular and Biomolecular*

*Spectroscopy* **2022**, *274*, 121094.

22. Sasikumar, T.; Ilanchelian, M., Colorimetric detection of hypochlorite based on the morphological changes of silver nanoprisms to spherical nanoparticles. *Analytical Methods* **2017**, *9* (21), 3151-3158.
23. Zaytsev, V. D.; Furletov, A. A.; Apyari, V. V.; Garshev, A. V.; Dmitrienko, S. G.; Zolotov, Y. A., Label-free silver triangular nanoplates for spectrophotometric determination of catecholamines and their metabolites. *Microchimica Acta* **2020**, *187* (11), 610.
24. Ma, X.; He, S.; Qiu, B.; Luo, F.; Guo, L.; Lin, Z., Noble Metal Nanoparticle-Based Multicolor Immunoassays: An Approach toward Visual Quantification of the Analytes with the Naked Eye. *ACS Sensors* **2019**, *4* (4), 782-791.
25. de la Rica, R.; Stevens, M. M., Plasmonic ELISA for the ultrasensitive detection of disease biomarkers with the naked eye. *Nature Nanotechnology* **2012**, *7* (12), 821-824.
26. Pham, X.-H.; Hahm, E.; Kim, T. H.; Kim, H.-M.; Lee, S. H.; Lee, Y.-S.; Jeong, D. H.; Jun, B.-H., Enzyme-catalyzed Ag Growth on Au Nanoparticle-assembled Structure for Highly Sensitive Colorimetric Immunoassay. *Scientific Reports* **2018**, *8* (1), 6290.
27. Wang, H.; Rao, H.; Luo, M.; Xue, X.; Xue, Z.; Lu, X., Noble metal nanoparticles growth-based colorimetric strategies: From monochrometric to multichrometric sensors. *Coordination Chemistry Reviews* **2019**, *398*, 113003.
28. Otsuki, J.; Sugawa, K.; Jin, S., Plasmonic triangular nanoprism sensors. *Materials Advances* **2021**, *2* (1), 32-46.
29. Parnklang, T.; Lertvachirapaiboon, C.; Pienpinijtham, P.; Wongravee, K.; Thammacharoen, C.; Ekgasit, S., H<sub>2</sub>O<sub>2</sub>-triggered shape transformation of silver nanospheres to nanoprisms with controllable longitudinal LSPR wavelengths. *RSC Advances* **2013**, *3* (31), 12886-12894.
30. Zhang, Q.; Hu, Y.; Guo, S.; Goebel, J.; Yin, Y., Seeded Growth of Uniform Ag Nanoplates with High Aspect Ratio and Widely Tunable Surface Plasmon Bands. *Nano Letters* **2010**, *10* (12), 5037-5042.
31. Zhang, Q.; Li, N.; Goebel, J.; Lu, Z.; Yin, Y., A systematic study of the synthesis of silver nanoplates: Is citrate a “magic” reagent? *Journal of the American Chemical Society* **2011**, *133*, 18931-18939.

32. Li, N.; Zhang, Q.; Quinlivan, S.; Goebel, J.; Gan, Y.; Yin, Y., H<sub>2</sub>O<sub>2</sub>-Aided Seed-Mediated Synthesis of Silver Nanoplates with Improved Yield and Efficiency. *ChemPhysChem* **2012**, *13* (10), 2526-2530.
33. Pollok, N. E.; Peng, Y.; Raj, N.; Walgama, C.; Crooks, R. M., Dual-shaped silver nanoparticle labels for electrochemical detection of bioassays. *ACS Applied Nano Materials* **2021**, *4* (10), 10764-10770.
34. Willets, K. A.; Van Duyne, R. P., Localized surface plasmon resonance spectroscopy and sensing. *Annual Review of Physical Chemistry* **2007**, *58* (1), 267-297.
35. Jana, J.; Ganguly, M.; Pal, T., Enlightening surface plasmon resonance effect of metal nanoparticles for practical spectroscopic application. *RSC Advances* **2016**, *6* (89), 86174-86211.
36. Mie, G., Beiträge zur Optik trüber Medien, speziell kolloidaler Metallösungen. *Annalen der Physik* **1908**, *330* (3), 377-445.
37. Gans, R., Über die Form ultramikroskopischer Goldteilchen. *Annalen der Physik* **1912**, *342* (5), 881-900.
38. Stockman, M. I., Nanoplasmonics: The physics behind the applications. *Physics Today* **2011**, *64* (2), 39-44.
39. Lea, M. C., Allotropic forms of silver. *American Journal of Science* **1889**, *s3-37* (222), 476-491.
40. Nowack, B.; Krug, H. F.; Height, M., 120 Years of Nanosilver History: Implications for Policy Makers. *Environmental Science & Technology* **2011**, *45* (4), 1177-1183.
41. Lee, S. H.; Jun, B.-H., Silver Nanoparticles: Synthesis and Application for Nanomedicine. *International Journal of Molecular Sciences* **2019**, *20* (4), 865.
42. Sharma, R. K.; Yadav, S.; Dutta, S.; Kale, H. B.; Warkad, I. R.; Zbořil, R.; Varma, R. S.; Gawande, M. B., Silver nanomaterials: synthesis and (electro/photo) catalytic applications. *Chemical Society Reviews* **2021**, *50* (20), 11293-11380.
43. Öztürk, İ.; Beğic, N.; Bener, M.; Apak, R., Antioxidant capacity measurement based on **K**-carrageenan stabilized and capped silver nanoparticles using green nanotechnology. *Journal of Molecular Structure* **2021**, *1242*, 130846.
44. Tsuji, T.; Iryo, K.; Watanabe, N.; Tsuji, M., Preparation of silver nanoparticles by

laser ablation in solution: influence of laser wavelength on particle size. *Applied Surface Science* **2002**, *202* (1), 80-85.

45. Navaladian, S.; Viswanathan, B.; Viswanath, R. P.; Varadarajan, T. K., Thermal decomposition as route for silver nanoparticles. *Nanoscale Research Letters* **2006**, *2* (1), 44.
46. Syafiuddin, A.; Salmiati; Salim, M. R.; Beng Hong Kueh, A.; Hadibarata, T.; Nur, H., A Review of Silver Nanoparticles: Research Trends, Global Consumption, Synthesis, Properties, and Future Challenges. *Journal of the Chinese Chemical Society* **2017**, *64* (7), 732-756.
47. Mirzaei, A.; Janghorban, K.; Hashemi, B.; Bonyani, M.; Leonardi, S. G.; Neri, G., Characterization and optical studies of PVP-capped silver nanoparticles. *Journal of Nanostructure in Chemistry* **2017**, *7* (1), 37-46.
48. Shrivastava, K.; Sahu, B.; Deb, M. K.; Thakur, S. S.; Sahu, S.; Kurrey, R.; Kant, T.; Patle, T. K.; Jangde, R., Colorimetric and paper-based detection of lead using PVA capped silver nanoparticles: Experimental and theoretical approach. *Microchemical Journal* **2019**, *150*, 104156.
49. Xue, C.; Mirkin, C. A., pH Switchable Silver Nanoprism Growth Pathways. *Angewandte Chemie* **2006**, *119* (12), 2082-2084.
50. Stefaniuk, T.; Wróbel, P.; Górecka, E.; Szoplik, T., Optimum deposition conditions of ultrasmooth silver nanolayers. *Nanoscale Research Letters* **2014**, *9* (1), 153.
51. Luo, X.; Chen, Y.; Yang, D.; Li, Z.; Han, Y., Morphology control of silver nanocrystals through a polyol synthesis. *Solid State Sciences* **2011**, *13* (9), 1719-1723.
52. Nasretdinova, G. R.; Fazleeva, R. R.; Mukhitova, R. K.; Nizameev, I. R.; Kadirov, M. K.; Ziganshina, A. Y.; Yanilkin, V. V., Electrochemical synthesis of silver nanoparticles in solution. *Electrochemistry Communications* **2015**, *50*, 69-72.
53. Rafique, M.; Sadaf, I.; Rafique, M. S.; Tahir, M. B., A review on green synthesis of silver nanoparticles and their applications. *Artificial Cells, Nanomedicine, and Biotechnology* **2017**, *45* (7), 1272-1291.
54. Abbasi, E.; Milani, M.; Fekri Aval, S.; Kouhi, M.; Akbarzadeh, A.; Tayefi Nasrabadi, H.; Nikasa, P.; Joo, S. W.; Hanifehpour, Y.; Nejati-Koshki, K.; Samiei, M.,

Silver nanoparticles: Synthesis methods, bio-applications and properties. *Critical Reviews in Microbiology* **2016**, *42* (2), 173-180.

55. Yaqoob, A. A.; Umar, K.; Ibrahim, M. N. M., Silver nanoparticles: various methods of synthesis, size affecting factors and their potential applications—a review. *Applied Nanoscience* **2020**, *10* (5), 1369-1378.

56. Ajitha, B.; Ashok Kumar Reddy, Y.; Sreedhara Reddy, P., Enhanced antimicrobial activity of silver nanoparticles with controlled particle size by pH variation. *Powder Technology* **2015**, *269*, 110-117.

57. Métraux, G. S.; Mirkin, C. A., Rapid Thermal Synthesis of Silver Nanoprisms with Chemically Tailorable Thickness. *Advanced Materials* **2005**, *17* (4), 412-415.

58. Aherne, D.; Ledwith, D. M.; Gara, M.; Kelly, J. M., Optical Properties and Growth Aspects of Silver Nanoprisms Produced by a Highly Reproducible and Rapid Synthesis at Room Temperature. *Advanced Functional Materials* **2008**, *18* (14), 2005-2016.

59. Jiang, X. C.; Chen, C. Y.; Chen, W. M.; Yu, A. B., Role of Citric Acid in the Formation of Silver Nanoplates through a Synergistic Reduction Approach. *Langmuir* **2010**, *26* (6), 4400-4408.

60. Jin, R.; Cao, Y.; Mirkin, C. A.; Kelly, K. L.; Schatz, G. C.; Zheng, J. G., Photoinduced Conversion of Silver Nanospheres to Nanoprisms. *Science* **2001**, *294* (5548), 1901-1903.

61. Ojea-Jiménez, I.; Romero, F. M.; Bastús, N. G.; Puentes, V., Small Gold Nanoparticles Synthesized with Sodium Citrate and Heavy Water: Insights into the Reaction Mechanism. *The Journal of Physical Chemistry C* **2010**, *114* (4), 1800-1804.

62. Tyagi, H.; Kushwaha, A.; Kumar, A.; Aslam, M., A Facile pH Controlled Citrate-Based Reduction Method for Gold Nanoparticle Synthesis at Room Temperature. *Nanoscale Research Letters* **2016**, *11* (1), 362.

63. Information, N. C. f. B., PubChem Compound Summary for CID 6224, Sodium Citrate. 2004.

64. Kilin, D. S.; Prezhdo, O. V.; Xia, Y., Shape-controlled synthesis of silver nanoparticles: Ab initio study of preferential surface coordination with citric acid. *Chemical Physics Letters* **2008**, *458* (1), 113-116.

65. Elghanian, R.; Storhoff, J. J.; Mucic, R. C.; Letsinger, R. L.; Mirkin, C. A., Selective

Colorimetric Detection of Polynucleotides Based on the Distance-Dependent Optical Properties of Gold Nanoparticles. *Science* **1997**, 277 (5329), 1078-1081.

66. Sarkar, S.; Das, R., Presence of chlorpyrifos shows blue shift of the absorption peak of silver nanohexagons solution – An indication of etching of nanocrystals and sensing of chlorpyrifos. *Sensors and Actuators B: Chemical* **2018**, 266, 149-159.
67. Liang, J.; Yao, C.; Li, X.; Wu, Z.; Huang, C.; Fu, Q.; Lan, C.; Cao, D.; Tang, Y., Silver nanoprism etching-based plasmonic ELISA for the high sensitive detection of prostate-specific antigen. *Biosensors and Bioelectronics* **2015**, 69, 128-134.
68. Zong, C.; Li, B.; Wang, J.; Liu, X.; Zhao, W.; Zhang, Q.; Nie, X.; Yu, Y., Visual and colorimetric determination of H<sub>2</sub>O<sub>2</sub> and glucose based on citrate-promoted H<sub>2</sub>O<sub>2</sub> sculpturing of silver nanoparticles. *Microchimica Acta* **2018**, 185 (3), 199.
69. Filippo, E.; Serra, A.; Manno, D., Poly(vinyl alcohol) capped silver nanoparticles as localized surface plasmon resonance-based hydrogen peroxide sensor. *Sensors and Actuators B: Chemical* **2009**, 138 (2), 625-630.
70. Vasileva, P.; Donkova, B.; Karadjova, I.; Dushkin, C., Synthesis of starch-stabilized silver nanoparticles and their application as a surface plasmon resonance-based sensor of hydrogen peroxide. *Colloids and Surfaces A: Physicochemical and Engineering Aspects* **2011**, 382 (1), 203-210.
71. Endo, T.; Yanagida, Y.; Hatsuzawa, T., Quantitative determination of hydrogen peroxide using polymer coated Ag nanoparticles. *Measurement* **2008**, 41 (9), 1045-1053.
72. Kaushal, S.; Nanda, S. S.; Samal, S.; Yi, D. K., Strategies for the development of metallic-nanoparticle-based label-free biosensors and their biomedical applications. *ChemBioChem* **2020**, 21 (5), 576-600.
73. Tran, H. V.; Nguyen, T. V.; Nguyen, L. T. N.; Hoang, H. S.; Huynh, C. D., Silver nanoparticles as a bifunctional probe for label-free and reagentless colorimetric hydrogen peroxide chemosensor and cholesterol biosensor. *Journal of Science: Advanced Materials and Devices* **2020**, 5 (3), 385-391.
74. Zuo, Y.; Chen, L.; Hu, X.; Wang, F.; Yang, Y., Silver nanoprism enhanced colorimetry for precise detection of dissolved oxygen. *Micromachines* **2020**, 11 (4), 383.
75. Lertvachirapaiboon, C.; Kiyokawa, I.; Baba, A.; Shinbo, K.; Kato, K., Colorimetric determination of hydrogen peroxide based on localized surface plasmon resonance of



- silver nanoprisms using a microchannel chip. *Analytical Letters* **2019**, *52*, 1939–1950.
76. Doan, V.-D.; Nguyen, V.-C.; Nguyen, T.-L.-H.; Nguyen, A.-T.; Nguyen, T.-D., Highly sensitive and low-cost colourimetric detection of glucose and ascorbic acid based on silver nanozyme biosynthesized by *Gleditsia australis* fruit. *Spectrochimica Acta Part A: Molecular and Biomolecular Spectroscopy* **2022**, *268*, 120709.
77. Wang, Y.; Cheng, C.; Ma, R.; Xu, Z.; Ozaki, Y., In situ SERS monitoring of intracellular H<sub>2</sub>O<sub>2</sub> in single living cells based on label-free bifunctional Fe<sub>3</sub>O<sub>4</sub>@Ag nanoparticles. *Analyst* **2022**, 1815-1823.
78. Karim, M. N.; Anderson, S. R.; Singh, S.; Ramanathan, R.; Bansal, V., Nanostructured silver fabric as a free-standing NanoZyme for colorimetric detection of glucose in urine. *Biosensors and Bioelectronics* **2018**, *110*, 8-15.
79. Huang, X.; Song, J.; Yung, B. C.; Huang, X.; Xiong, Y.; Chen, X., Ratiometric optical nanoprobe enable accurate molecular detection and imaging. *Chemical Society Reviews* **2018**, *47* (8), 2873-2920.
80. Haber, J.; Sokolov, K., Synthesis of Stable Citrate-Capped Silver Nanoprisms. *Langmuir* **2017**, *33* (40), 10525-10530.
81. Kelly, K. L.; Coronado, E.; Zhao, L. L.; Schatz, G. C., The Optical Properties of Metal Nanoparticles: The Influence of Size, Shape, and Dielectric Environment. *The Journal of Physical Chemistry B* **2003**, *107* (3), 668-677.
82. Wongravee, K.; Parnklang, T.; Pienpinijtham, P.; Lertvachirapaiboon, C.; Ozaki, Y.; Thammacharoen, C.; Ekgasit, S., Chemometric analysis of spectroscopic data on shape evolution of silver nanoparticles induced by hydrogen peroxide. *Physical Chemistry Chemical Physics* **2013**, *15* (12), 4183-4189.
83. Liu, D.; Yang, J.; Wang, H.-F.; Wang, Z.; Huang, X.; Wang, Z.; Niu, G.; Hight Walker, A. R.; Chen, X., Glucose Oxidase-Catalyzed Growth of Gold Nanoparticles Enables Quantitative Detection of Attomolar Cancer Biomarkers. *Analytical Chemistry* **2014**, *86* (12), 5800-5806.
84. Nitinaivinij, K.; Parnklang, T.; Thammacharoen, C.; Ekgasit, S.; Wongravee, K., Colorimetric determination of hydrogen peroxide by morphological decomposition of silver nanoprisms coupled with chromaticity analysis. *Analytical Methods* **2014**, *6*,

9816–9824.

85. Espinoza, M. G.; Hinks, M. L.; Mendoza, A. M.; Pullman, D. P.; Peterson, K. I., Kinetics of Halide-Induced Decomposition and Aggregation of Silver Nanoparticles. *The Journal of Physical Chemistry C* **2012**, *116* (14), 8305-8313.
86. Bian, S.-D.; Jia, J.-H.; Wang, Q.-M., High-Nuclearity Silver Clusters Templated by Carbonates Generated from Atmospheric Carbon Dioxide Fixation. *Journal of the American Chemical Society* **2009**, *131* (10), 3422-3423.
87. Patrito, E. M.; Olivera, P. P., Adsorption of carbonate species on silver. I. Nature of the surface bond. *Electrochimica Acta* **1998**, *44* (6), 1237-1245.
88. Chudobova, D.; Nejd, L.; Gumulec, J.; Krystofova, O.; Rodrigo, M. A. M.; Kynicky, J.; Ruttkay-Nedecky, B.; Kopel, P.; Babula, P.; Adam, V.; Kizek, R., Complexes of Silver(I) Ions and Silver Phosphate Nanoparticles with Hyaluronic Acid and/or Chitosan as Promising Antimicrobial Agents for Vascular Grafts. *International Journal of Molecular Sciences* **2013**, *14* (7), 13592-13614.
89. Wang, Z.; Gupta, R. K.; Luo, G.-G.; Sun, D., Recent Progress in Inorganic Anions Templated Silver Nanoclusters: Synthesis, Structures and Properties. *The Chemical Record* **2020**, *20* (5), 389-402.
90. Agus, E.; Voutchkov, N.; Sedlak, D. L., Disinfection by-products and their potential impact on the quality of water produced by desalination systems: A literature review. *Desalination* **2009**, *237* (1-3), 214-237.
91. Quiñones, O.; Snyder, S. A.; Cotruvo, J. A.; Fisher, J. W., Analysis of bromate and bromide in blood. *Toxicology* **2006**, *221* (2), 229-234.
92. Polo, A. M. S.; Lopez-Peñalver, J. J.; Rivera-Utrilla, J.; Von Gunten, U.; Sánchez-Polo, M., Halide removal from waters by silver nanoparticles and hydrogen peroxide. *Science of The Total Environment* **2017**, *607-608*, 649-657.
93. Kim, U.-J.; Kannan, K., Method for the Determination of Iodide in Dried Blood Spots from Newborns by High Performance Liquid Chromatography Tandem Mass Spectrometry. *Analytical Chemistry* **2018**, *90* (5), 3291-3298.
94. Forman, H. J.; Bernardo, A.; Davies, K. J. A., What is the concentration of hydrogen peroxide in blood and plasma? *Archives of Biochemistry and Biophysics* **2016**, *603*, 48-53.

95. Krishnan, J.; Subhash, N. N.; Muraleedharan, C. V.; Mohanan, P. V.; Nandakumar, M.; Neethu, S.; Rethnagireeshwar, R., Chitra disinfection gateway for the management of COVID-19 in public entry places. *Transactions of the Indian National Academy of Engineering* **2020**, *5* (2), 289-294.
96. Park, J.; Kim, J. W.; Kim, H.; Yoon, W., An electrochemical hydrogen peroxide sensor for applications in nuclear industry. *Nuclear Engineering and Technology* **2021**, *53* (1), 142-147.
97. Scaramuzza, N.; Cigarini, M.; Mutti, P.; Berni, E., Sanitization of packaging and machineries in the food industry: Effect of hydrogen peroxide on ascospores and conidia of filamentous fungi. *International Journal of Food Microbiology* **2020**, *316*, 108421.
98. Vasconcelos, H.; Matias, A.; Mendes, J.; Araújo, J.; Dias, B.; Jorge, P. A. S.; Saraiva, C.; de Almeida, J. M. M. M.; Coelho, L. C. C., Compact biosensor system for the quantification of hydrogen peroxide in milk. *Talanta* **2022**, 124062.
99. EFSA Panel on Nutrition, N. F.; Allergens, F.; Turck, D.; Castenmiller, J.; de Henauw, S.; Hirsch-Ernst, K.-I.; Kearney, J.; Knutsen, H. K.; Maciuk, A.; Mangelsdorf, I.; McArdle, H. J.; Pelaez, C.; Pentieva, K.; Siani, A.; Thies, F.; Tsbouri, S.; Vinceti, M.; Aggett, P.; Fairweather-Tait, S.; Martin, A.; Przyrembel, H.; de Sesmaisons-Lecarré, A.; Naska, A., Dietary reference values for chloride. *EFSA Journal* **2019**, *17* (9), e05779.
100. Guo, Y.; Compton, R. G., A bespoke chloride sensor for seawater: Simple and fast with a silver electrode. *Talanta* **2021**, *232*, 122502.
101. Chowdhury, S.; Koyappathody, T. M. F.; Karanfil, T., Removal of halides from drinking water: technological achievements in the past ten years and research needs. *Environmental Science and Pollution Research* **2022**, *29* (37), 55514-55527.



จุฬาลงกรณ์มหาวิทยาลัย  
**CHULALONGKORN UNIVERSITY**

## VITA

**NAME** Charles Oliver Avenido

**DATE OF BIRTH** 19 January 1990

**PLACE OF BIRTH** Manila

**INSTITUTIONS ATTENDED** Bicol University (2016 -2010)

**HOME ADDRESS** 316 Bucalbucalan, Sorsogon City, Sorsogon, 4700  
Philippines

**PUBLICATION** Avenido, C.O.; Wongravee, K.; Srisa-Art, M.; Development  
of an Enzyme-Free Hydrogen Peroxide Sensor  
Using Dual-Shaped Silver Nanoparticles. In 48th  
International Congress on Science, Technology and  
Technology-Based Innovation (STT48), Nakhon Si  
Thammarat, Thailand, November 29-December 1, 2022;  
pp 701-709

**AWARD RECEIVED** Graduate Scholarship Program for ASEAN or Non-ASEAN  
Countries.